

Norihiro Watanabe, Guido Blöcher, Mauro
Cacace, Sebastian Held, Thomas Kohl

Geoenergy Modeling III: Enhanced Geothermal Systems

13th October 2016

Springer

About the Authors

Dr.-Ing. Norihiro Watanabe is a postdoctoral researcher in the department of Environmental Informatics at the Helmholtz Centre for Environmental Research – UFZ in Leipzig, Germany. He studied civil engineering and environmental science at Okayama University in Japan for his Bachelor and Master degrees, and received his doctoral degree in engineering from Dresden University of Technology in Germany. His research interest is in developing numerical models for coupled thermal-hydraulic-mechanical-chemical processes in fractured rocks for various geotechnical applications such as deep geothermal systems and underground waste disposals.

Dr. Guido Blöcher is currently working as a scientist at the Helmholtz Centre Potsdam – GFZ German Research Centre for Geosciences in Potsdam, Germany. After his graduation in Hydrogeology and Engineering he was employed as a project leader in hydrogeology by Geotec Consult GbR Bochum until 2004. In November 2004 he started his Ph.D. at the GFZ German Research Centre for Geosciences. He received his Ph.D. for improved understanding of hydraulic and mechanical interactions in porous media; identification of mechanical and hydraulic properties depending on pore space geometry and reconstruction of pore space geometry within the context of geothermal energy. Since 2008 he is employed as a Post-Doc at the German Research Centre for Geosciences in Potsdam within the content of geothermal energy and aquifer thermal energy storage. During his Ph.D. and as a Post-Doc, Dr. Blöcher had lectured at the Faculty VI Planning, Construction & Environment at Technical University of Berlin, Germany.

Dr. Mauro Cacace is a senior associate scientist at the Helmholtz Centre Potsdam – GFZ German Research Centre for Geosciences in Potsdam, Germany. After graduated in Physics at the University in Milan, Italy, he obtained his doctoral degree in Earth Sciences at the Free University in Berlin by developing numerical methods to simulate viscous-plastic lithospheric deformation mechanisms at plate boundaries and in the interior of stable

continents. His research focuses on understanding the physical processes responsible for the occurrence of distinct rock material behaviors at different spatio-temporal scales, fluid-rock interaction mechanisms, and their effects on the thermo-mechanical state of natural and engineered reservoirs by combining laboratory experiments and numerical modeling techniques.

Sebastian Held is currently doing his Ph.D. at the Karlsruhe Institute of Technology (KIT) in Karlsruhe, Germany. He graduated in Applied Geosciences at the KIT working during his Master thesis on numerical-economical coupled description of an EGS. During his Ph.D. at the Division of Geothermics at the KIT he works on multidisciplinary geothermal exploration using geophysical and geochemical techniques to characterize a geothermal reservoir in the Andes of Southern Chile.

Prof. Dr. Thomas Kohl is leading the division of geothermal energy research at the Institute for Applied Geosciences of the Karlsruhe Institute of Technology, KIT, and is head of the Helmholtz geothermal program at KIT. Starting with his degree in Geophysics he became research associate at CNRS in Paris in the field of seismology and got his PhD at ETH Zurich in 1992. After his habilitation he was director of the ETH spin-off company GEOWATT AG until 2011. His FE code FRACTure was widely applied to characterize coupled T-H-M processes in fractured rock. He collaborated in numerous national, international and European research projects and directed many geothermal projects. The major research interest at KIT is on the investigation of reservoir-scale aspects in fractured subsurface systems during the assessment and operation of a geothermal reservoir. As author of more > 70 reviewed manuscripts in renowned journals he was awarded with the H. J. Ramey Award of GRC in 2015. His research division is supported by EnBW Energie Baden-Württemberg AG and includes today 15 PhD and postdoc scientists.

Preface

This tutorial presents the introduction of the open-source software *Open-GeoSys* (*OGS*) for enhanced geothermal reservoir modeling. The material is mainly based on several national training courses at the Helmholtz Centre for Environmental Research – UFZ in Leipzig, the GFZ German Research Centre for Geosciences in Potsdam, Germany but also international training courses on the subject held in Guangzhou, China in 2013. The Soultz-sous-Forêts case study was kindly provided by Sebastian Held and Thomas Kohl at the Karlsruhe Institute of Technology (KIT), Germany. This tutorial is also the result of a close cooperation within the *OGS* community (www.opengeosys.org). These voluntary contributions are highly acknowledged.

The book contains general information regarding enhanced geothermal reservoir modeling and step-by-step model set-up with *OGS* and the open-source mesh generation software *MeshIt* developed by Guido Blöcher and Mauro Cacace at GFZ. Two benchmark examples and two case studies are presented in details.

This book is intended primarily for graduate students and applied scientists, who deal with geothermal system analysis. It is also a valuable source of information for professional geoscientists wishing to advance their knowledge in numerical modeling of geothermal processes including thermal convection processes. As such, this book will be a valuable help in training of geothermal modeling.

There are various commercial software tools available to solve complex scientific questions in geothermics. This book will introduce the user to an open source numerical software code for geothermal modeling which can even be adapted and extended based on the needs of the researcher.

This tutorial is the third volume in a series that will represent further applications of computational modeling in energy sciences. Within this series, the planned tutorials related to the specific simulation platform OGS are:

- Geoenergy Modeling I. Geothermal Processes in Fractured Porous Media, Böttcher et al. (2015), DOI 10.1007/978-3-319-31335-1, <http://www.springer.com/de/book/9783319313337>,
- Geoenergy Modeling II. Shallow Geothermal Systems, Shao et al. (2016, in press),
- Geoenergy Modeling III. Enhanced Geothermal Systems, Watanabe et al. (2016), this volume,
- Computational Geotechnics: Storage of Energy Carriers, Nagel et al. (2017*),
- Models of Thermochemical Heat Storage, Lehmann et al. (2017*).

These contributions are related to a similar publication series in the field of environmental sciences, namely:

- Computational Hydrology I: Groundwater flow modeling, Sachse et al. (2015), DOI 10.1007/978-3-319-13335-5, <http://www.springer.com/de/book/9783319133348>,
- Computational Hydrology II, Sachse et al. (2016, in press),
- OGS Data Explorer, Rink et al. (2017*)

(*publication time is approximated).

Leipzig, July 2016
Potsdam, July 2016

Karlsruhe, July 2016

Norihiro Watanabe
Guido Blöcher
Mauro Cacace
Sebastian Held
Thomas Kohl

Acknowledgements

We deeply acknowledge the *OpenGeoSys* community for their continuous support to the *OpenGeoSys* development activities. We would like to express our sincere thanks to HIGRADE in providing funding the *OpenGeoSys* training course at the Helmholtz Centre for Environmental Research. We also would like to thank Leslie Jakobs for proofreading.

We are grateful to Dr. Hang Si from the WIAS Institute in Berlin for extending TetGen regarding our demands. Without the collaboration the superimposing of 1D well paths would not be achieved by now.

We would like to thank the owner of Soultz data, GEIE Exploitation Minière de la Chaleur for providing Soultz reservoir data, especially hydraulic data and data of well completion of GPK1 – GPK4.



Contents

1	Introduction	1
1.1	Geothermal Energy	1
1.2	Enhanced Geothermal Systems – EGS	2
1.3	Reservoir Modeling	5
2	Theory	9
2.1	Conceptual Model	9
2.2	Mathematical Model	11
2.3	Numerical Solution	14
3	Open-Source Software	17
3.1	OpenGeoSys – OGS	17
3.2	MeshIt	19
4	Benchmarks	23
4.1	2D Hot Dry Rock Benchmark	23
4.2	2D Hot Sedimentary Aquifer benchmark	39
5	Case Study: Groß Schönebeck	49
5.1	Site Description	49
5.2	Model Setup	53
5.3	Mesh Generation	54
5.4	Simulation of Initial Reservoir Conditions	64
5.5	Simulation of Heat Extraction Process	74
6	Case Study: Soultz-sous-Forêts	79
6.1	Site Description	79
6.2	Model Setup	82
6.3	Simulation of Initial Reservoir Conditions	86
6.4	Simulation of Heat Extraction Process	95
A	Keywords	99

References 105

Chapter 1

Introduction

Welcome to the third volume of the Geoenergy Modeling series. This volume will introduce the reader to the field of modeling enhanced geothermal reservoirs. In the beginning chapter, we will briefly introduce Enhanced Geothermal Systems (EGS) and its reservoir modeling.

1.1 Geothermal Energy

Geothermal energy is a promising renewable energy source which can be found anywhere and is not affected by climate changes. Its resource potential is enormously large as the total heat content of the Earth is of the order of 12.6×10^{24} MJ and that of the crust is the order of 5.4×10^{21} MJ (Dickson and Fanelli, 2004), compared to the world electricity generation 7.1×10^{13} MJ in 2007 (International Energy Agency, 2009). However, accessibility to the resource is limited with current technology, and only a fraction of the resource has been exploited so far.

Geothermal energy originates from the formation of the Earth and the radioactive decay of materials in the Earth's mantle and crust. Heat is continuously supplied to the surface from the Earth's interior, i.e. subsurface temperatures increase with depth (Fig. 1). The average geothermal gradient in the upper crust is around $30 \text{ }^\circ\text{C}/\text{km}$ and at a depth of 5 km, temperatures reach $150 \text{ }^\circ\text{C}$. As shown in Fig. 1, some areas benefiting from favorable geothermal conditions due to volcanic activities and natural convection see higher temperatures closer to the surface.

The first electricity generation from the geothermal energy was made in Larderello, Italy in 1904 when Prince Ginori Conti powered his 3/4-horsepower reciprocating steam engine at his factory (DiPippo, 2012). Since then, geothermal power has been relying mostly on hydrothermal resources which can be found near continental plate boundaries and volcanoes where heated fluids are available near-surface (Fig. 2). Countries having such fa-

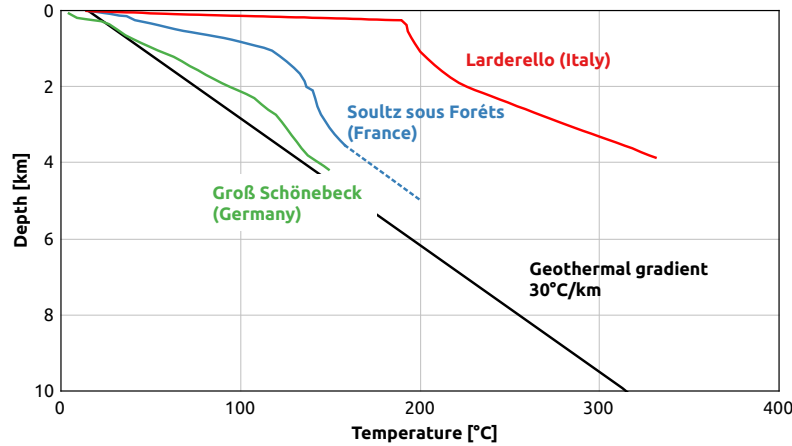


Fig. 1: Examples of temperature profile with the depth

favorable geological conditions are for example the United States, Philippines, Indonesia, Mexico, New Zealand, and Iceland. The United States has the installed capacity of 3.5 GW, which is about 27% of the world installed capacity of 12.6 GW in 2015. In some countries like Iceland, Philippines, the geothermal power supplies more than 25% of the nation's electricity.

1.2 Enhanced Geothermal Systems – EGS

1.2.1 Concept

Conventional hydrothermal systems are somewhat limited in their locations, although the heat is stored everywhere in the Earth's crust. In order to increase accessible geothermal resources, tremendous research efforts over the last decades have been devoted to developing Enhanced Geothermal Systems (EGS). EGS are aimed at creating or enhancing heat exchangers in deep and low permeable hot rocks where natural hydrothermal systems do not exist or are not productive enough for an economic use. Thus, EGS enable the exploitation of more resources with fewer constraints on geological conditions.

The idea of EGS originated from Hot Dry Rock (HDR) systems proposed at the Los Alamos National Laboratory in 1970. HDR concept targets very low permeable hot rocks where little fluid is present, and is based on stimulation of geothermal wells for generating artificial fracture networks where heat transfer media, i.e. fluid, can be circulated (Fig. 3). Later, the concept was extended to EGS which target other geological conditions and existing low productive hydrothermal systems.

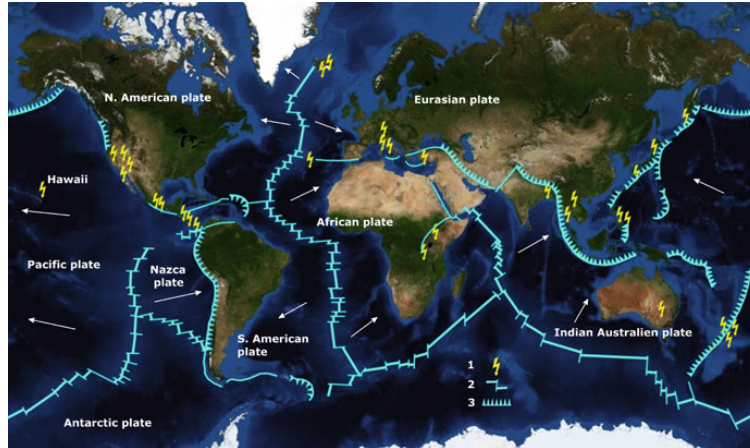


Fig. 2: World pattern of plates, oceanic ridges, oceanic trenches, subduction zones, and geothermal fields. Arrows show the direction of movement of the plates towards the subduction zones. (1) Geothermal fields producing electricity; (2) mid-oceanic ridges crossed by transform faults (long transversal fractures); (3) subduction zones, where the subducting plate bends downwards and melts in the asthenosphere (Böttcher et al (2016) after Dickson and Fanelli (2004))

1.2.2 Stimulation

The key technology of EGS is the stimulation of wellbores for generating fluid pathways. Stimulation techniques can be classified as (1) hydraulic stimulation including hydraulic fracturing and hydraulic shearing, (2) thermal stimulation, and (3) chemical stimulation (Huenges, 2010). Hydraulic stimulation can improve the field up to several hundreds of meters away from the borehole, whereas chemical and thermal stimulation have impacts up to a distance of few tens of meters.

Hydraulic fracturing generates new fractures or opens existing fractures by tensile stress due to injection of fluid at a pressure higher than the minimum principal stress. Depending on rock permeability, a favorable working fluid is selected, e.g. water or cross-linked gels. Water is used for low permeable rocks and often produces long fractures in the range of a few hundred meters. For a wide range of formations with varying permeability, the gels including proppants or sands can be used for the stimulation. These generated fractures have a length of about 50 - 100 m (Huenges, 2010).

Hydraulic shearing reactivates existing fractures favorably oriented for shearing caused by increased pore pressure in the fractures. Shear displace-

¹ Image:https://commons.wikimedia.org/wiki/File:Geothermie_Prinzip.svg

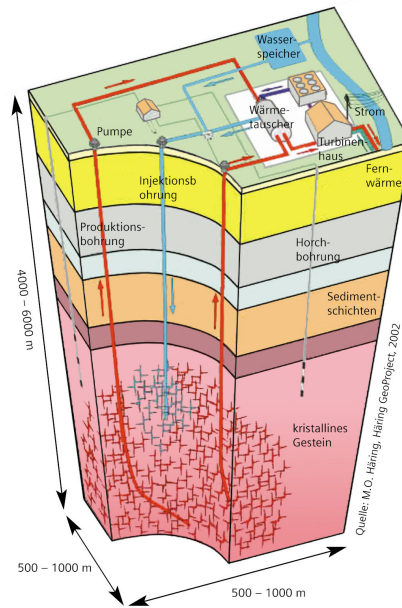


Fig. 3: Hot Dry Rock system ¹

ment along the fracture planes results in self-propping dilatation and permeability increase. The method is effective for impermeable rocks having pre-existing fracture networks.

Thermal stimulation is based on the injection of cold water into high-temperature rocks, which results in thermal contraction of the rocks and creates or enhances fractures near the borehole. Chemical stimulation is based on acidic treatments to remove clogging of pore spaces or enhance fracture permeability in the vicinity of boreholes. For further details of the stimulation techniques, please refer to Huenges (2010).

1.2.3 EGS Types

Depending on geological conditions and presence of natural hydrothermal systems, different types of EGS can be developed. Typical examples are as follows (DiPippo, 2012)

- Hot Dry Rock (HDR)
- Enhanced Hydrothermal Systems (EHS)
- Hot Sedimentary Aquifers (HSA)

As explained above, the HDR type targets formations consisting of high temperature but very low permeable rocks (e.g. granite). To extract heat from the formations, fluid pathways have to be generated or enhanced by hydraulic fracturing or hydraulic shearing. Examples of the HDR sites are Fenton Hill (USA), Rosemanowes (UK), and Hijiori (Japan).

The EHS type targets natural hydrothermal systems whose productivity is insufficient for an economic use. Stimulation methods should be applied for increase of reservoir permeability. This kind of EGS can be found, for example, in Soultz-sous-Forêts (France).

The HSA type is aimed at exploiting permeable and fluid-saturated formations at the depth of a few kilometers. Often these regions do not have strong geothermal gradients, and the fluid temperature is low to moderate (e.g. 120-150°C), which can still be used in binary power stations. Examples of this type are Groß Schönebeck (Germany), Neustadt-Glewe (Germany).

1.3 Reservoir Modeling

1.3.1 Objectives

Modeling of enhanced geothermal reservoirs is an essential tool for efficient and sustainable utilization of the geothermal resources. The simulation allows us to understand hydraulic and heat transport processes in the reservoir (i.e. heat extraction process), which is necessary to assess the geothermal potential and to define the optimum exploitation and plant operation strategies for a specific site (Franco and Vaccaro, 2014; O’Sullivan et al, 2001). Furthermore, environmental impacts of EGS are not well known yet. Their long-term influences have to be further investigated with the help of reservoir modeling. Due to geological complexity and the number of physical processes involved, numerical methods, e.g. the finite difference method (FDM), the finite volume method (FVM), and the finite element method (FEM), have been widely used for geothermal reservoir modeling (Zyvoloski et al, 1988).

Primary goals of reservoir modeling are history matching and prediction of future scenarios. History matching means adjustment of the reservoir model

to observed field data (e.g. temperature log, pumping tests, tracer tests) to determine reservoir parameters (in-situ temperature distribution, petrophysical properties of rocks, regional flow fields, etc). The validated model can further be used as a basis for prediction of future scenarios. The prediction is aimed at evaluating efficiency and productivity of the systems with varying extraction and injection strategies (e.g. extraction rates, reinjection temperatures, wellbore locations, installation of induced fractures). Optimum exploitation and operation strategies can be discussed based on the simulation results (Franco and Vaccaro, 2014).

1.3.2 Workflow

Practical workflow of the reservoir simulation is illustrated in Fig. 4. The first step is the construction of a geological model based on the field data such as borehole logs, core samples, and geophysical measurements. Important for the reservoir modeling is the selection and evaluation of major geological features (i.e. geological layers, fault zones, and fractures) influencing the system hydraulics.

The second step is the generation of a mesh (or a computation grid) which represents spatial structures of the selected geological model and also controls accuracy of simulation results. Some geological modeling software such as Petrel can directly export a structurally gridded mesh. For a geometrically complex reservoir, an unstructured mesh may be preferred because it can represent geometry more accurately. An unstructured mesh can be generated based on geometric data from the geological model. Available software for the unstructured meshing are, for example, Gmsh (Geuzaine and Remacle, 2009), Hypermesh (Altair Engineering, Inc.), MeshIt (Cacace and Blöcher, 2015), and Tetgen (Si, 2015).

The third step is the parameterization of the reservoir model, i.e. determining material properties as well as initial and boundary conditions. Material properties include thermo-physical properties for geological units, discrete fractures, fault zones. Key parameters for the reservoir modeling are, for example, permeability, porosity, rock density, rock specific heat, and rock thermal conductivity. Initial and boundary conditions are set according to the regional circumstances (e.g. in-situ temperature distribution, terrestrial heat flux, regional groundwater flow field).

After generating a mesh and assigning reservoir parameters, numerical simulation can be executed. A stepwise readjustment of the geological model or reservoir parameters is required until a good agreement with the field data is obtained. In any case a sensitivity analysis investigating the effects of each parameters has to be made to determine the validity of the model. For productivity predictions, one can set up different numerical models to compare scenarios, e.g. effects of additional induced fractures.

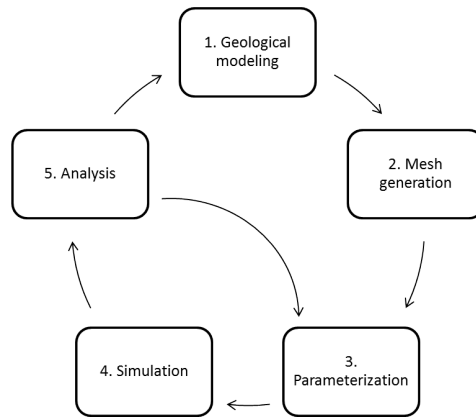


Fig. 4: Workflow of the reservoir modeling

As geological input data are subject to uncertainties, evaluation of reliability of the simulation results is an important task during numerical modeling. In-situ data, sufficient for model evaluation, are limited due to financial or technical issues. Typically available data are point or line data from core samples and wellbore logging, and scattered data from geophysical measurements (e.g. microseismic monitoring). Thus quantification of data uncertainties using stochastic methods such as Monte-Carlo simulation is important for reservoir analysis to evaluate the simulated results (Kolditz et al, 2010; Watanabe et al, 2010).

Chapter 2

Theory

This chapter briefly glances at the basic theory of enhanced geothermal reservoir modeling, specifically hydraulic and thermal processes in fractured geological systems, and their numerical solutions with the finite element method.

2.1 Conceptual Model

We start with conceptual modeling of flow and transport processes in EGS geothermal reservoirs. As illustrated in Fig. 1, enhanced geothermal reservoirs often consist of the following features

- geological units (rock matrices)
- pre-existing fractures
- fault zones
- induced fractures
- wellbores
- geothermal fluids

Heat, which is our primary interest, is stored in both rocks and geothermal fluids. We assume fluids are in a liquid phase in the reservoir because of a high pressure at the depth of a few kilometers. Pre-existing fractures and fault zones can be highly permeable and often govern the flow pathways in the underground system. Wellbores are drilled into the formations to produce heated geothermal fluids and to reinject cooled fluid. Fluid can flow into/from a wellbore through its open-hole sections. Induced fractures are created as a result of the wellbore stimulation for enhancing the fluid transmissivity in the system.

To conceptualize the reservoir for flow and heat transport modeling, we consider it as a composition of multiple representative elementary volumes (REV), i.e. *porous media* and *discrete fractures* as shown in Fig. 2. In addition

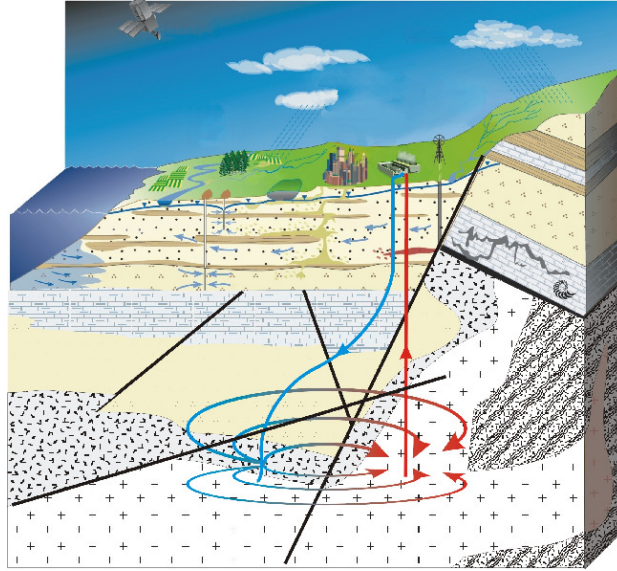


Fig. 1: Illustration of an enhanced geothermal system with faulted subsurface structures (McDermott, 2006)

to the physical processes within each REV, interactions between the REVs have to be taken into account.

Porous media represent rock matrices without fractures or highly fractured rocks. The term rock matrix denotes a quite heterogeneous medium at a microscopic scale which is interweaved by numerous microfissures and pores. It is assumed, however, that these microstructures are well connected, and thus, the hydraulic and transport characteristics of the rock matrix can be described by averaged quantities (Kolditz, 1997). Highly fractured rocks can also be homogenized as equivalent porous media. Alternatively, one can consider it as dual-continua consisting of two homogeneous subsystems, e.g. one for fractures and the other one for the rock matrix (Barenblatt et al, 1960).

Discrete fractures represent macroscopic fractures which are sparsely distributed at a scale of interest and are not suited for homogenization. These fractures provide the most likely pathway for the transmission of fluid, contaminants, and heat through the geologic underground.

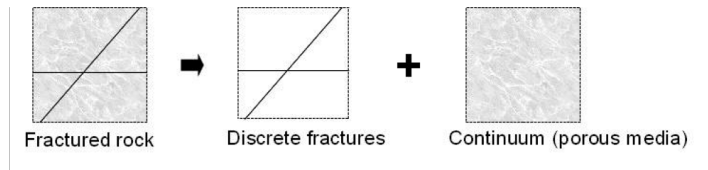


Fig. 2: Combination of porous media and discrete fractures

2.2 Mathematical Model

Mathematical expressions of liquid flow and heat transport processes in porous media and discrete fracture are briefly presented. Their governing equations can be derived from macroscopic balance laws for mass and energy in the media. The corresponding field variables are liquid phase pressure p [Pa] and temperature T [K]. Details of the mathematical models can be found in literature such as Guvanasen and Chan (2000); Kohl et al (1995); Noorishad and Tsang (1996); Rutqvist and Stephansson (2003).

Porous media

We consider porous media consisting of a liquid phase and a solid phase. Local thermodynamic equilibrium is assumed between the phases. The volume fraction of liquid phase in the media is given by the porosity n [-].

Based on mass balance equations of both liquid and solid phases, liquid flow in porous media can be expressed in the following volume balance equation

$$S_m \frac{\partial p}{\partial t} + \nabla \cdot \mathbf{q}_m = 0 \quad (1)$$

where S_m is the constrained specific storage of the medium [1/Pa] and \mathbf{q}_m is the Darcy velocity in the media [m/s]. The specific storage comprises a mechanical alteration in response to pressure and can be given as $S_m = (1 - n)/K^s + n/K^l$ with the bulk modulus of solid K^s and of liquid K^l [Pa]. The Darcy velocity is given as

$$\mathbf{q}_m = \frac{\mathbf{k}}{\mu} (-\nabla p + \rho^l \mathbf{g}) \quad (2)$$

where \mathbf{k} is the intrinsic permeability tensor [m²], μ is the fluid dynamic viscosity [Pa s], ρ^l is the fluid density [kg/m³], and \mathbf{g} is the gravitational acceleration vector [m/s²].

Diffusive and advective heat transport in porous media can be expressed from the energy balance law as

$$\rho c_p \frac{\partial T}{\partial t} + \nabla \cdot (-\boldsymbol{\lambda} \nabla T + \rho^l c_p^l \mathbf{q}_m) = 0 \quad (3)$$

where $c_p \rho$ is the effective heat capacity of porous media [J/m³/K], $\boldsymbol{\lambda}$ is the effective thermal conductivity tensor of media, and c_p^l is the specific heat capacity [J/kg/K] of liquid. Both the heat capacity and the thermal conductivity of porous media can be estimated as an arithmetic mean of each phase property weighted by its volume fraction, i.e.

$$c_p \rho = n c_p^l \rho^l + (1 - n) c_p^s \rho^s \quad (4)$$

$$\boldsymbol{\lambda} = n \lambda^l \mathbf{I} + (1 - n) \boldsymbol{\lambda}^s \quad (5)$$

with \mathbf{I} the identity tensor. For the effective thermal conductivity, other kinds of averaging methods such as harmonic or geometric mean may be used if the information about a spatial layout of the phases is available.

Discrete fractures

Fractures can be idealized as a parallel plate with the mechanical aperture (the width) b [m]. It is assumed that physical processes occur mainly along the fracture and fluid pressure and temperature are uniform across the fracture width. The assumption may be invalid if the fracture is filled with some low permeable materials. For simplicity, we also ignore the distinction between mechanical and hydraulic apertures.

Liquid flow in discrete fractures can be given as the following volume balance equation along the fracture

$$b S_f \frac{\partial p}{\partial t} + \nabla \cdot (b \mathbf{q}_f) = 0 \quad (6)$$

where $S_f = \alpha/K^l$ is the specific storage of a fracture, and \mathbf{q}_f is the flow velocity in the fracture defined as

$$\mathbf{q}_f = \frac{b^2}{12\mu} (-\nabla p + \rho^l \mathbf{g}) \quad (7)$$

from the cubic law (Snow, 1969; Zimmerman and Bodvarsson, 1996). The heat transport equation in discrete fractures is

$$b \rho^l c_p^l \frac{\partial T}{\partial t} + \nabla \cdot b (-\lambda^l \nabla T + \rho^l c_p^l \mathbf{q}_f T) = 0 \quad (8)$$

describing volumetric energy balance of the liquid filling the fractures.

Coupling between porous media and discrete fractures

Fluid and heat flux should be exchanged between porous media and discrete fractures. One of the simplest approaches implementing the exchanges is to impose continuity conditions of pressure and temperature along the boundary of porous media and fractures. Alternatively one can explicitly consider exchange fluxes as explained in Segura and Carol (2004).

Boundary conditions

In order to specify the solution for the above equations, one needs to prescribe boundary conditions along all boundaries. For the liquid flow equations, the following boundary conditions are available:

- Prescribed pressure [Pa] (Dirichlet condition)

$$p = \bar{p} \quad \text{on} \quad \Gamma_p \quad (9)$$

for imposing hydrostatic conditions at domain boundaries or pressure at wellbores.

- Prescribed fluid flux [m/s] (Neumann condition)

$$q_n = \mathbf{q} \cdot \mathbf{n} \quad \text{on} \quad \Gamma_q \quad (10)$$

with the normal vector \mathbf{n} for imposing inflow or outflow rate at wellbores as well as regional flow conditions at domain boundaries.

- Fluid transfer [m/s] (Robin condition)

$$q_n = h_p(p - p_\infty) \quad \text{on} \quad \Gamma_{hp} \quad (11)$$

with the transfer coefficient h [m/Pa/s] for including flux exchange with a surrounding aquifer. The coefficient may be approximately calculated by $h = k/(\mu d)$ where k is the permeability in rocks between the aquifers, μ is the fluid viscosity, and d is the distance to the surrounding aquifer [m].

For the heat transport equations, the following boundary conditions are often used for deep geothermal modeling:

- Prescribed temperature [K] (Dirichlet condition)

$$T = \bar{T} \quad \text{on} \quad \Gamma_T \quad (12)$$

for imposing natural thermal gradients at model boundaries and temperature of injected fluid.

- Prescribed heat flux [W/m²] (Neumann condition)

$$j_n = \mathbf{j}_{\text{diff}} \cdot \mathbf{n} \quad \text{on} \quad \Gamma_j \quad (13)$$

with the diffusive heat flux \mathbf{j}_{diff} for imposing terrestrial heat flux.

2.3 Numerical Solution

The above governing equations can be numerically solved using the finite element method (FEM) for space and the finite different method (FDM) for time. The FEM is chosen in this study because the method is suitable for handling non-uniform complex geometries.

In FEM, geometric objects can be represented by a mesh of 1-D, 2-D and/or 3-D basic elements (geometric units) such as lines, triangles, quadrilaterals, tetrahedrons, hexahedra and pyramids. For enhanced geothermal reservoir modeling, one can combine multiple element types in different dimensions (Fig. 3, Table 1). Discrete fractures can be idealized as lower-dimensional geometric objects, e.g. triangles in three-dimensional space. Wellbore open-hole sections can be represented by one-dimensional objects, e.g. lines in three-dimensional space. To implement the continuity conditions of variables at the boundary of porous media and fractures, one must locate fracture elements along edges of porous medium elements, and make both kinds of elements share the same nodes (Segura and Carol, 2004; Woodbury and Zhang, 2001).

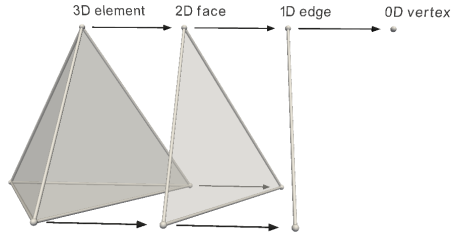


Fig. 3: Elements with different spatial dimensions (Cacace and Blöcher, 2015)
2

Based on a decomposed space (i.e. a mesh), spatial distributions of primary variables $p(\mathbf{x}, t)$ and $T(\mathbf{x}, t)$ can be approximated with their nodal values and basis functions constructed from shape functions of mesh elements as

$$p^h(\mathbf{x}, t) = \mathbf{N}(\mathbf{x})\mathbf{P}(t) \quad (14a)$$

$$T^h(\mathbf{x}, t) = \mathbf{N}(\mathbf{x})\mathbf{T}(t) \quad (14b)$$

² Reprinted from *Environmental Earth Sciences*, MeshIt – a software for three dimensional volumetric meshing of complex faulted reservoirs, Vol. 74(6), 2015, pp. 5191–5209, Cacace M, Blöcher G, with permission from Springer.

Space	Porous media	Discrete fractures	Wellbores
2D	triangle, quadrilateral	line	point
3D	tetrahedral, hexahedral, prismatic, pyramid	triangle, quadrilateral	line

Table 1: Element types for enhanced geothermal reservoir modeling

where \mathbf{P} and \mathbf{T} are nodal value vectors for the unknowns, and \mathbf{N} is the shape function row vector.

As a result of FEM discretization, one can obtain the following time ordinal differential equations (ODEs).

$$\mathbf{M}_H \dot{\mathbf{P}} + \mathbf{K}_H \mathbf{P} = \mathbf{f}_H \quad (15a)$$

$$\mathbf{M}_T \dot{\mathbf{T}} + \mathbf{K}_T \mathbf{T} = \mathbf{f}_T \quad (15b)$$

where \mathbf{P} and \mathbf{T} are vectors of nodal fluid pressure and temperature, respectively. \mathbf{M} and \mathbf{K} are process-specific mass and transport matrices. \mathbf{f} is a vector including the source/sink terms. Details of the matrices and vectors are given as follows:

$$\mathbf{M}_H = \sum_{e \in \Omega} \int_{\Omega_e} \mathbf{N}^T S_m \mathbf{N} \, d\Omega + \sum_{e \in \Gamma_d} \int_{\Gamma_e} \mathbf{N}^T b S_f \mathbf{N} \, d\Gamma \quad (16a)$$

$$\mathbf{K}_H = \sum_{e \in \Omega} \int_{\Omega_e} \nabla \mathbf{N}^T \frac{\mathbf{k}}{\mu} \nabla \mathbf{N} \, d\Omega + \sum_{e \in \Gamma_d} \int_{\Gamma_e} \nabla \mathbf{N}^T \frac{b^3}{12\mu} \nabla \mathbf{N} \, d\Gamma \quad (16b)$$

$$\begin{aligned} \mathbf{f}_H &= \sum_{e \in \Omega} \int_{\Omega_e} \nabla \mathbf{N}^T \frac{\mathbf{k}}{\mu} \rho^l \mathbf{g} \, d\Omega - \int_{\Gamma_q} \mathbf{N}^T q_n \, d\Gamma \\ &\quad + \sum_{e \in \Gamma_d} \int_{\Omega_e} \nabla \mathbf{N}^T \frac{b^3}{12\mu} \rho^l \mathbf{g} \, d\Omega - \int_{\Sigma_q} \mathbf{N}^T q_n \, d\Sigma \end{aligned} \quad (16c)$$

$$\mathbf{M}_T = \sum_{e \in \Omega} \int_{\Omega_e} \mathbf{N}^T \rho c_p \mathbf{N} \, d\Omega + \sum_{e \in \Gamma_d} \int_{\Gamma_e} \mathbf{N}^T b \rho^l c_p^l \mathbf{N} \, d\Gamma \quad (16d)$$

$$\begin{aligned} \mathbf{K}_T &= \sum_{e \in \Omega} \left(\int_{\Omega_e} \mathbf{N}^T \rho^l c_p^l \mathbf{q}_m \nabla \mathbf{N} \, d\Omega + \int_{\Omega_e} \nabla \mathbf{N}^T \lambda \nabla \mathbf{N} \, d\Omega \right) \\ &\quad + \sum_{e \in \Gamma_d} \left(\int_{\Gamma_e} \mathbf{N}^T b \rho^l c_p^l \mathbf{q}_f \nabla \mathbf{N} \, d\Gamma + \int_{\Gamma_e} \nabla \mathbf{N}^T b \lambda_l \nabla \mathbf{N} \, d\Gamma \right) \end{aligned} \quad (16e)$$

$$\mathbf{f}_T = - \int_{\Gamma_j} \mathbf{N}^T j_n \, d\Gamma - \int_{\Sigma_j} \mathbf{N}^T j_n \, d\Sigma \quad (16f)$$

Time discretization of the ODEs is accomplished through the first order finite difference scheme. We use the backward Euler method as

$$\left[\frac{1}{\Delta t} \mathbf{M}_H + \mathbf{K}_H \right] \mathbf{P}_{n+1} = \frac{1}{\Delta t} \mathbf{M}_H \mathbf{P}_n + \mathbf{f}_H \quad (17a)$$

$$\left[\frac{1}{\Delta t} \mathbf{M}_T + \mathbf{K}_T \right] \mathbf{T}_{n+1} = \frac{1}{\Delta t} \mathbf{M}_T \mathbf{T}_n + \mathbf{f}_T \quad (17b)$$

where Δt is a time step size [s] and subscripts $n + 1$ and n denotes current and previous time step values.

The above two equations are coupled via the flow velocity and the material parameters. For example, the fluid density and viscosity strongly depends on temperature so that results of the heat transport equation influence the groundwater flow equation. To solve the coupled problems, we follow the partitioned approach which iteratively solves individual problem until the solutions converge. If the coupling effects are strong, one may need to decrease time step sizes to obtain the convergence.

Chapter 3

Open-Source Software

Software used in the later benchmark examples and case studies are introduced. All of them are open-source and freely available for scientific research purposes.

- OpenGeoSys – A numerical framework for solving THM/C problems in porous and fractured media (Kolditz et al (2012), <http://www.opengeosys.org>). Please note that we use a modified version of OpenGeoSys for this tutorial. Its source code is available from <http://norihiro-w.github.io/ogs5-egs>.
- MeshIt – A software for three dimensional volumetric meshing of complex faulted reservoirs (Cacace and Blöcher, 2015). To get the software, please contact bloech@gfz-potsdam.de or cacace@gfz-potsdam.de.
- Gmsh – A general purpose mesh generator (<http://gmsh.info>)
- GMSH2OGS – A mesh file converter from Gmsh to OGS formats (<https://docs.opengeosys.org/download>)
- ParaView – A 3D visualization software (<http://www.paraview.org>)

In the following sections, we briefly glance at OpenGeoSys and MeshIt.

3.1 OpenGeoSys – OGS

3.1.1 *Concept*

OGS is a scientific, open-source initiative for the numerical simulation of thermo-hydro-mechanical/chemical (THMC) processes in porous and fractured media, continuously developed since the mid-1980s. The OGS code targets primarily applications in environmental geoscience, e.g. in the fields of contaminant hydrology, water resources management, waste deposits, or geothermal systems, but it has also been applied to new topics in energy storage.

OGS is participating several international benchmarking initiatives, e.g. DECOVALEX (with applications mainly in waste repositories), CO2BENCH (CO₂ storage and sequestration), SeSBENCH (reactive transport processes) and HM-Intercomp (coupled hydrosystems).

The basic concept is to provide a flexible numerical framework (using primarily the FEM) for solving coupled multi-field problems in porous-fractured media. The software is written with an object-oriented (C++) FEM concept including a broad spectrum of interfaces for pre- and postprocessing. To ensure code quality and to facilitate communications among different developers worldwide OGS is outfitted with professional software-engineering tools such as platform-independent compiling and automated result testing tools. A large benchmark suite has been developed for source code and algorithm verification over time. Heterogeneous or porous-fractured media can be handled by dual continua or discrete approaches, i.e. by coupling elements of different dimensions. OGS has a built-in, random-walk particle tracking method for Euler-Lagrange simulations. The code has been optimized for massive parallel machines. The OGS Toolbox concept promotes (mainly) open-source code coupling e.g. to geochemical and biogeochemical codes such as iPHREEQC, GEMS, and BRNS for open functionality extension. OGS also provides continuous workflows including various interfaces for pre- and post-processing. Visual data integration has become an important tool for establishing and validating data driven models (OGS DataExplorer). The OGS software suite provides three basic modules for data integration, numerical simulation and 3D visualization.

3.1.2 Input Files

The numerical simulation with OGS relies on file-based model setups, which means each model needs different input files that contain information on specific aspects of the model. All the input files share the same base name but have a unique file ending, with which the general information of the file can already be seen. For example, a file with ending `.pcs` provides the information of the process involved in the simulation such as groundwater flow or Richards flow; whereas in a file with ending `.ic` the initial condition of the model can be defined. Tab. 1 gives an overview and short explanations of the *OGS* input files needed for one of the benchmarks.

The basic structure and concept of an input file is illustrated in examples in the following benchmark chapters. As we can see, an input file begins with a main keyword which contains sub-keywords with corresponding parameter values. If an input file ends with the keyword `#STOP`, everything written after file input terminator `#STOP` is unaccounted for input. Please also refer to the *OGS* input file description in the Appendix and the keyword description to the *OGS* webpage (<http://www.opengeosys.org/help/documentation>)

Table 1: *OGS* input files for heat transport problems

Object	File	Explanation
GEO	<code>file.gli</code>	system geometry
MSH	<code>file.msh</code>	finite element mesh
PCS	<code>file.pcs</code>	process definition
NUM	<code>file.num</code>	numerical properties
TIM	<code>file.tim</code>	time discretization
IC	<code>file.ic</code>	initial conditions
BC	<code>file.bc</code>	boundary conditions
ST	<code>file.st</code>	source/sink terms
MFP	<code>file.mfp</code>	fluid properties
MSP	<code>file.mfp</code>	solid properties
MMP	<code>file.mmp</code>	medium properties
OUT	<code>file.out</code>	output configuration

3.2 MeshIt

3.2.1 Concept

MeshIt is a three-dimensional software for generating high quality, boundary conforming Delaunay tetrahedral meshes suitable for Finite Element (FEM) or Finite Volume (FVM) thermal-hydraulic-mechanical-chemical (THMC) dynamic simulations of complex faulted and fractured reservoir applications. MeshIt provides the users with an open source, time efficient, robust and “easy to handle” software tool to bridge the gap between static 3D geological model representation of the underground and dynamic forward models of flow and transport processes especially targeting reservoir domains comprising fault zones, natural and induced fracture systems, wells (open hole section).

The main goal of MeshIt is to generate consistent, detailed watertight Piecewise Linear Complex (PLC) as based on realistic 3D geological models, with a specific orientation for faulted and fractured reservoirs. Based on the input geological model, MeshIt will also automatically calculate all required intersection and internal constraints to be added to the PLC.

Another major advantage of MeshIt, when compared to existing solutions, is that it offers the possibility to combine in a final quality tetrahedral mesh, geological features of different dimensions. Those comprise: 0D vertices representing local sources or sinks, 1D polylines representing the open-hole sections of operating wells, 2D triangulated surfaces representing fault zones and fractures, and 3D volumetric elements representing the reservoir formations. A constrained, boundary conforming, Delaunay tetrahedralization is performed on the generated PLC which results in a high-quality unstructured tetrahedral mesh suitable for dynamic forward FE/FV numerical simulations.

The crucial factor that makes the software applicable for real case reservoir applications is that it enables fast and efficient modification of the system geometry as soon as new geological information is available. At the same time, parallel computing guarantees time efficiency thus enabling the handling of large datasets. With the single exception of the final constrained Delaunay tetrahedralization, all routines have been written for parallel computation on symmetric multiprocessing computer (SMP) architecture, as based on the Qt thread support environment via platform-independent threading classes.

The software comes with an integrated Graphical User Interface (GUI) that it is meant to facilitate the user in accomplishing the different stages required for the meshing workflow. All instructions are provided by the user interactively via the GUI or passed in the form of text files.

3.2.2 Workflow

Workflow using MeshIt are divided into the following steps:

1. Pre-meshing
2. Selection of the final model geometry
3. Meshing

Pre-meshing reconstructs the 3D topology of all surfaces from point data provided by the user. The reconstruction is achieved by 1) calculation of convex hulls, 2) triangulation of all reconstructed surfaces, and 3) calculation of surface-surface intersections.

After having the reconstructed surfaces including all the intersections, the user has to define the domain of interest to be discretized. Via the programming interface, the user can interactively select segments of both convex hulls and internal polylines, which will be used to bound areas to be triangulated for each surface. The selected constraints for each surface, once combined, will provide the essential geometric parts of the planar straight line graph (PSLG) of each surface that can be used to carry out a constrained conforming Delaunay triangulation of the resulting graph. As a last step of selecting the final model geometry, the user assigns the proper region IDs to 1D wells, 2D fractures, and 3D geological units.

The last step is volume meshing with a constrained Delaunay tetrahedralization of the PLC. The tetrahedralization is carried out as based on the meshing libraries provided by the open source software *Tetgen* (Si, 2015). After the constrained Delaunay tetrahedralization, the resulting mesh is handled by MeshIt. Each tetrahedron is marked by its own region ID, while faults and wells are represented by marked tetrahedrons' faces and edges respectively.

3.2.3 Supported file formats

The native input file format required by MeshIt consists of input data defined by pointwise surfaces. Wells and surfaces, the latter representing fault zone, fracture systems and stratigraphic horizons of a reservoir are defined in external files consisting of unsorted triplets of x-, y-, z-coordinates. Supported formats are either non-ordered text or comma separated nodal values or fully unstructured VTU grids. Additionally, an importing interface to existing commercial geological modeling software (e.g. Paradigm GoCad, Earth Vision, Petrel, and Geomodeller) has been supplemented to read and format volume-based geological representations.

The final 3D mesh can be exported either for pure visualization purposes or to be used as input for FE/FV numerical simulations. For visualization, ParaView is fully supported. In addition, existing interfaces to commercial and open source THMC dynamic simulators are also available, including COMSOL Multiphysics, FEFLOW (ver. 7), Moose, and OpenGeoSys.

Chapter 4

Benchmarks

This chapter presents several benchmark examples for demonstrating basics of how to set up *OpenGeoSys* input files for EGS reservoir modeling and check simulation results mainly using *ParaView*. Meshes are prepared using *Gmsh*. Readers can find more benchmark examples in the following materials

- Geoenery Modeling I: Geothermal Processes in Fractured Porous Media (Böttcher et al, 2016)
- THMC benchmark books (vol.1–3) (Kolditz et al, 2012, 2015)
- OGS community webpage (www.opengeosys.org)

4.1 2D Hot Dry Rock Benchmark

Problem Definition

As an example of Hot Dry Rock (HDR) type EGS reservoirs, this benchmark simulates heat extraction from a hot granite rock where an artificial fracture is created for fluid circulation (Fig. 1). The reservoir is located at a depth of 4 km and its in-situ temperature is 200 °C. The vertical fracture has a square shape with an edge length of 300 m. A doublet system is installed with two wellbores separated by a distance of 150 m.

The geothermal reservoir can be simplified to a horizontal 2D model as illustrated in Fig. 2. We consider a scenario of circulating water at a rate of 1 L/s. The temperature of the injected water is 70°C. Water exists in liquid phase in the reservoir because of high pressure. Properties of the rock matrix, the hydraulic fracture and fluid are listed in Table 1. Fracture permeability was determined by the Cubic law (Snow, 1969). Fluid viscosity is considered as temperature dependent (Ramey et al, 1974),

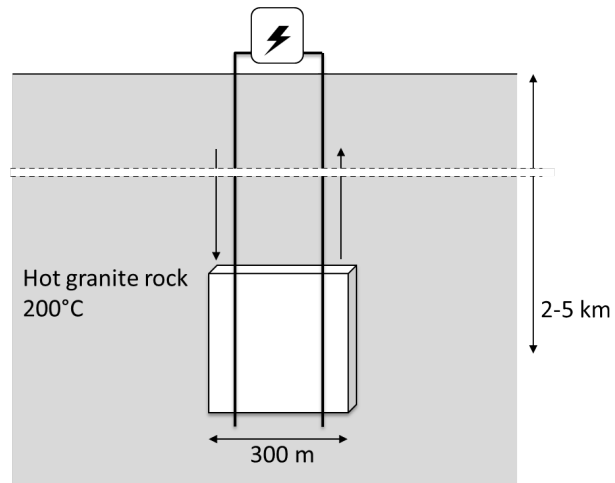


Fig. 1: Benchmark 1: Concept

$$\mu = 2.394 \cdot 10 \left[\frac{248.37}{T + 133.15} \right] \cdot 10^{-5} \quad (1)$$

where temperature T is in Celsius.

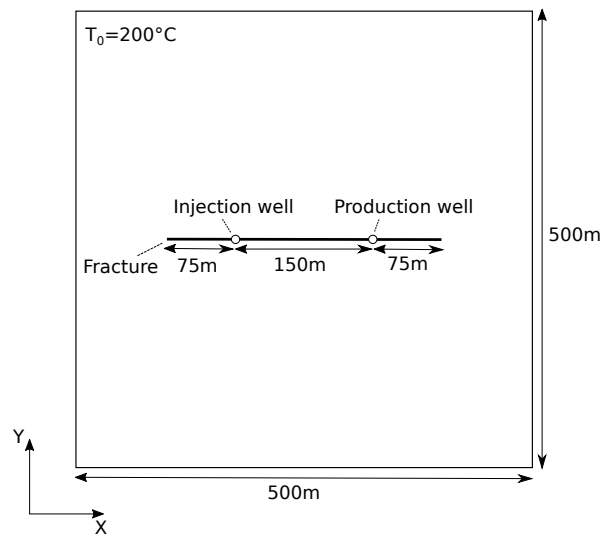


Fig. 2: Benchmark 1: Geometric layout

Property	Value
Initial reservoir temperature	200 °C
Initial reservoir pore pressure	10 MPa
Production rate	1 L/s
Injection rate	1 L/s
Injection temperature	70 °C
Fracture horizontal length	300 m
Fracture vertical length	300 m
Fracture mean aperture	100 μ m
Fracture permeability	$8.3333 \cdot 10^{-10}$ m ²
Fracture porosity	100 %
Fracture storage	$4 \cdot 10^{-10}$ Pa ⁻¹
Distance between the wells	150 m
Rock permeability	10^{-17} m ²
Rock porosity	1 %
Rock density	2600 kg/m ³
Rock specific heat capacity	950 J/kg/K
Rock thermal conductivity	3.0 W/m/K
Rock storage	10^{-10} Pa ⁻¹
Fluid density	1000 kg/m ³
Fluid viscosity	Ramey et al (1974)
Fluid specific heat capacity	4200 J/kg/K
Fluid thermal conductivity	0.65 W/m/K

Table 1: Benchmark 1: Parameters

OGS Input Files

The first example is very simple except for a mesh file which will be generated using Gmsh software and the mesh file converter. Other files can be created manually with a Text editor. We recommend starting with geometry (GLI) and mesh (MSH) files. Input files for the benchmark are available from <https://docs.openegeosys.org/books/geoenergy-modeling-iii>.

GLI - geometry

Before creating FEM parameters, we prepare geometric objects which are used later to assign boundary conditions and result output. The following geometric objects are needed in this example,

Listing 4.1: GLI input file

```
#POINTS
0 0 0 0
1 500 0 0
2 500 500 0
3 0 500 0
4 175 250 0 $NAME POINT_IN
5 325 250 0 $NAME POINT_OUT
#POLYLINE
```

```

$NAME
PLY_OUTER
$POINTS
0
1
2
3
0
#STOP

```

MSH - finite element mesh

Mesh (MSH) files contain data about the finite element mesh(es) such as nodes and elements. In addition to geometrical data, element data include the associated material group (see MMP file). In this example, we use an automatic finite element mesh generator GMSH to discretize the domain. The matrix (material ID 0) and the fracture (material ID 1) are discretized with 2D triangular elements and 1D line elements, respectively. The following GMSH input file (`ex_hdr.geo`) describes the model geometry as well as the material grouping. The variables `lc` and `lc2` control mesh refinement near the domain boundary and the fracture, respectively.

Listing 4.2: GMSH input file (`ex_hdr.geo`)

```

Mesh.Algorithm = 1;
Mesh.Optimize = 1;
lc=50;
lc2=10;
Point(0)={0,0,0,lc};
Point(1)={500,0,0,lc};
Point(2)={500,500,0,lc};
Point(3)={0,500,0,lc};
Point(4)={100,250,0,lc2};
Point(5)={400,250,0,lc2};
Point(6)={175,250,0,lc2};
Point(7)={325,250,0,lc2};
Line (1) = {0,1};
Line (2) = {1,2};
Line (3) = {2,3};
Line (4) = {3,0};
Line (5) = {4,6};
Line (6) = {6,7};
Line (7) = {7,5};
Line Loop(1) = {1,2,3,4};
Ruled Surface(1) = {1};
Line {5} In Surface {1};
Line {6} In Surface {1};
Line {7} In Surface {1};
Point {6} In Surface {1};
Point {7} In Surface {1};
Physical Surface(1) = {1};
Physical Line(2) = {6, 5, 7};

```

After preparing the text file, run the following commands to execute Gmsh and convert a created mesh file to an OGS mesh file.

```
> gmsh ex_hdr.geo -2 -o ex_hdr.gmsh.msh
> GMSH20GS -i ex_hdr.gmsh.msh -o ex_hdr.msh
```

The generated mesh is shown in Fig. 3. The corresponding MSH input file will be like below.

Listing 4.3: MSH input file

```
#FEM_MSH
$PCS_TYPE
NO_PCS
$NODES
417 // The number of nodes
0 0 0 0 // Node ID, x, y, z coordinates
1 500 0 0
2 500 500 0
...
$ELEMENTS
823 // The number of elements
0 1 line 4 44 // Element ID, material ID, element type, node IDs
1 1 line 44 45
...
#STOP
```

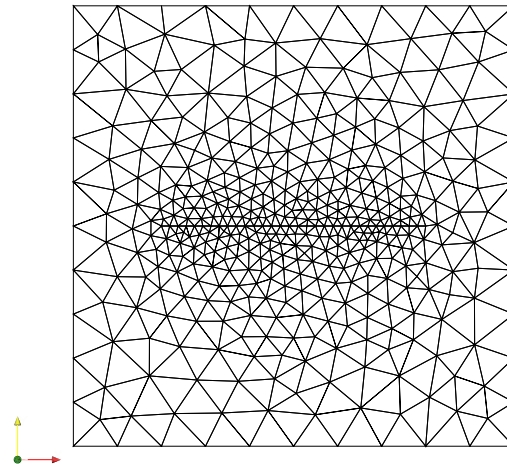


Fig. 3: Benchmark 1: An example mesh created by Gmsh

PCS - process definition

Process (PCS) files (Table 1) specify the physico-biochemical process being simulated. OGS is a fully coupled THMC (thermo-hydro-mechanical-chemical) simulator, therefore, a large variety of process combination is available with subsequent dependencies for OGS objects. The following example defines the liquid flow and heat transport processes being simulated. Only steady state is calculated in the liquid flow process.

Listing 4.4: PCS input file

```
#PROCESS
$PCS_TYPE
  LIQUID_FLOW
#PROCESS
$PCS_TYPE
  HEAT_TRANSPORT
#STOP
```

NUM - numerical properties

The next set of two files (NUM and TIM) are specifying numerical parameters, e.g. for spatial and temporal discretization as well as parameters for equation solvers. Numerics (NUM) files (Table 1) contain information for numerical settings such as linear/nonlinear/coupling solvers, time collocation, and the number of Gauss integration points. The process subkeyword (`$PCS_TYPE`) specifies the process to whom the numerical parameters belong to (e.g. `HEAT_TRANSPORT`). The linear solver subkeyword (`$LINEAR_SOLVER`) then determines the parameters for the linear equation solver. It should be noted that the modified OGS version uses Lis (Library of Iterative Solvers for linear systems, www.ssisc.org/lis, Nishida (2010)) for linear solution. The following example specifies using the GMRES solver (Lis solver type 9) and the ILU preconditioner (Lis preconditioner type 2) with the error tolerance of 10^{-12} for both the liquid flow and heat transport processes. The coupling control subkeyword (`$COUPLING_CONTROL`) specifies a convergence tolerance for primary variables of the process in coupling iterations. The two processes need to be iteratively solved until solutions converge because they interact each other through temperature-dependent fluid viscosity. The following example specifies an absolute tolerance of 10 Pa for pressure and 10^{-3} for temperature. `LMAX` means the maximum norm is used for coupling errors. In addition, the coupling iteration keyword `$OVERALL_COUPLING` needs to be specified at the beginning of the file.

Listing 4.5: NUM input file

```
$OVERALL_COUPLING
;min_iter -- max_iter
```

```

1          25
#NUMERICS
$PCS_TYPE
  LIQUID_FLOW
$LINEAR_SOLVER
; method error_tolerance max_iterations theta precondition storage
  9          0 1.e-012          1000          1.0 2          4
$COUPLING_CONTROL
;error method -- tolerances
  LMAX 10
#NUMERICS
$PCS_TYPE
  HEAT_TRANSPORT
$LINEAR_SOLVER
; method error_tolerance max_iterations theta precondition storage
  9          0 1.e-012          1000          1.0 2          4
$COUPLING_CONTROL
;error method -- tolerances
  LMAX 1.e-3
#STOP

```

TIM - time discretization

Time discretization (TIM) files (Table 1) specify the time stepping schemes for related processes. The following example specifies a uniform subdivision of the simulation period 30 years by 360 (i.e. one month for each time step) for both the liquid flow and heat transport process. Note that seconds is used as a unit of time.

Listing 4.6: TIM input file

```

#TIME_STEPPING
$PCS_TYPE
  LIQUID_FLOW
$TIME_START
  0.0
$TIME_END
  946080000 ; 30 years
$TIME_STEPS
  360 2628000 ; 1 month
#TIME_STEPPING
$PCS_TYPE
  HEAT_TRANSPORT
$TIME_START
  0.0
$TIME_END
  946080000
$TIME_STEPS
  360 2628000
#STOP

```

IC - initial conditions

The next set of files (IC/BC/ST) are specifying initial and boundary conditions as well as source and sink terms for related processes. The following example applies a initial condition value 10 MPa for the primary variable pressure in the liquid flow process for the entire domain and 200 °C for the primary variable temperature in the heat transport process. Note that Kelvin is used as a unit of temperature in OGS input files in this tutorial.

Listing 4.7: IC input file

```
#INITIAL_CONDITION
$PCS_TYPE
  LIQUID_FLOW
$PRIMARY_VARIABLE
  PRESSURE1
$GEO_TYPE
  DOMAIN
$DIS_TYPE
  CONSTANT 10e6 // unit Pa
#INITIAL_CONDITION
$PCS_TYPE
  HEAT_TRANSPORT
$PRIMARY_VARIABLE
  TEMPERATURE1
$GEO_TYPE
  DOMAIN
$DIS_TYPE
  CONSTANT 473.15 // unit K
#STOP
```

BC - boundary conditions

The boundary conditions (BC) file (Table 1) assigns the boundary conditions to the model domain. The following example applies a constant Dirichlet boundary condition 10 MPa for the liquid flow process for the primary variable pressure at the domain boundary with name `PLY_OUTER`. For the primary variable temperature in the heat transport process, it applies constant Dirichlet boundary condition values 200 °C and 70 °C at the domain boundary and at the point with name `POINT_IN`, respectively. Note that BC objects are linked to geometry objects (here `POINT` and `POLYLINE`).

Listing 4.8: BC input file

```
#BOUNDARY_CONDITION
$PCS_TYPE
  LIQUID_FLOW
$PRIMARY_VARIABLE
  PRESSURE1
$GEO_TYPE
  POLYLINE PLY_OUTER
$DIS_TYPE
  CONSTANT 10e6
```

```

#BOUNDARY_CONDITION
$PCS_TYPE
HEAT_TRANSPORT
$PRIMARY_VARIABLE
TEMPERATURE1
$GEO_TYPE
POLYLINE PLY_OUTER
$DIS_TYPE
CONSTANT 473.15
#BOUNDARY_CONDITION
$PCS_TYPE
HEAT_TRANSPORT
$PRIMARY_VARIABLE
TEMPERATURE1
$GEO_TYPE
POINT POINT_IN
$DIS_TYPE
CONSTANT 343.15
#STOP

```

ST - source/sink terms

The source/sink term (ST) file (Table 1) assigns the source and sink term and the Neumann type boundary conditions to the model domain. The following example applies an injection rate of 1 L/s (10^{-3} m³/s) for the liquid flow process for the primary variable pressure at the point with name POINT_IN and an production rate of 1 L/s at the point with name POINT_OUT. Note that a negative sign is used for outward flux.

Listing 4.9: ST input file

```

#SOURCE_TERM
$PCS_TYPE
LIQUID_FLOW
$PRIMARY_VARIABLE
PRESSURE1
$GEO_TYPE
POINT POINT_IN
$DIS_TYPE
CONSTANT 1e-3 // unit m3/s
#SOURCE_TERM
$PCS_TYPE
LIQUID_FLOW
$PRIMARY_VARIABLE
PRESSURE1
$GEO_TYPE
POINT POINT_OUT
$DIS_TYPE
CONSTANT -1e-3
#STOP

```

MFP - fluid properties

The fluid properties (MFP) file (Table 1) defines the material properties of the fluid phase(s). For multi-phase flow models we have multiple fluid properties objects. It contains physical parameters such as fluid density ρ^f , dynamic fluid viscosity μ such as heat capacity c^f , and thermal conductivity λ^f . The first parameter for the material properties is the material model number.

Listing 4.10: MFP input file

```
#FLUID_PROPERTIES
$DENSITY
1 1000.0
$VISCOSITY
22 ; Ramey (1974)
$SPECIFIC_HEAT_CAPACITY
1 4200.0
$HEAT_CONDUCTIVITY
1 0.65
#STOP
```

MSP - solid properties

The solid properties (MSP) file (Table 1) defines the material properties of the solid phase. It contains physical parameters such as solid density ρ^s , thermophysical parameters such as thermal expansion coefficient β_T^s , heat capacity c^s , and thermal conductivity λ^s . The first parameter for the material properties is the material model number.

Listing 4.11: MSP input file

```
#SOLID_PROPERTIES
$DENSITY
1 2600
$THERMAL
EXPANSION
1e-005
CAPACITY
1 950
CONDUCTIVITY
1 3.0
#SOLID_PROPERTIES
$DENSITY
1 2600
$THERMAL
EXPANSION
1e-005
CAPACITY
1 950.0
CONDUCTIVITY
1 3.0
#STOP
```

MMP - porous medium properties

The medium properties (MMP) file (Table 1) defines the material properties of the porous medium for all processes (single continuum approach). It contains geometric properties related to the finite element dimension (geometry dimension and area) as well as physical parameters such as porosity n , specific storage S_s , tortuosity τ , and permeability tensor \mathbf{k} . The following example includes definitions of the rock matrix properties and the fracture properties. The reservoir thickness of 300 m is specified in `$GEOMETRY_AREA`. For the fracture, the geometry area should also include its aperture 100 μm , i.e. (the geometry area) = (the reservoir depth) \times (the fracture aperture).

Listing 4.12: MMP input file

```
#MEDIUM_PROPERTIES
$GEOMETRY_DIMENSION
  2
$GEOMETRY_AREA
  300 // unit m
$POROSITY
  1 0.01
$PERMEABILITY_TENSOR
  ISOTROPIC 1e-17
$STORAGE
  1 1e-10
#MEDIUM_PROPERTIES
$GEOMETRY_DIMENSION
  1
$GEOMETRY_AREA
  3e-2 ; aperture 100 micro m
$POROSITY
  1 1.0
$PERMEABILITY_TENSOR
  ISOTROPIC 8.3333e-10
$STORAGE
  1 4e-10
#STOP
```

OUT - output parameters

The output (OUT) file (Table 1) specifies output of simulation results. A user has to provide output value names on which geometry, at which times, and in which file format. The following output file contains three output objects, first, output of data in the entire domain at every 10 time steps in ParaVewData (PVD) format, second, output of data at the point `POINT_IN` at each time step in CSV format, and third, output of data at the point `POINT_OUT` at each time step in CSV format.

Listing 4.13: OUT input file

```
#OUTPUT
$NOD_VALUES
```

```

PRESSURE1
TEMPERATURE1
$ELE_VALUES
VELOCITY1_X
VELOCITY1_Y
$MFP_VALUES
DENSITY
VISCOSITY
$GEO_TYPE
DOMAIN
$DAT_TYPE
PVD
$TIM_TYPE
STEPS 10
#OUTPUT
$NOD_VALUES
PRESSURE1
TEMPERATURE1
$GEO_TYPE
POINT POINT_IN
$DAT_TYPE
CSV
$TIM_TYPE
STEPS 1
#OUTPUT
$NOD_VALUES
PRESSURE1
TEMPERATURE1
$GEO_TYPE
POINT POINT_OUT
$DAT_TYPE
CSV
$TIM_TYPE
STEPS 1
#STOP

```

Run OGS

After having all the input files completed you can run your first simulation. It is recommended to copy the OGS executable (`ogs.exe` on Windows, `ogs` on Mac/Linux) into the working directory, where the input files are located.

Open your favorite terminal window (the command prompt on Windows) and move to the working directory. Execute `ogs` followed by the project name `ex_hdr`.

```

> cd (a path to the working directory)
> ogs ex_hdr &> log.txt

```

The simulation may take a few minutes. Result files will be created in the working directory.

Tips

- Executing OGS with `&> log.txt` writes all the log messages into a text file `log.txt`. Having the log file is helpful when you want to check details of simulations, e.g. if there is any error occurred during simulations.

Visualization

With the above input files, OGS will generate the following result files

Result file name(s)	Description of the file
<code>ex_hdr_*.vtu</code>	Series of Visualization Toolkit (VTK) data files at different time steps
<code>ex_hdr.pvd</code>	A ParaView Data (PVD) file containing a list of the VTU files with time step information
<code>ex_hdr_time_POINT_IN.csv</code>	A CSV file containing temporal values at the point named <code>POINT_IN</code>
<code>ex_hdr_time_POINT_OUT.csv</code>	A CSV file containing temporal values at the point named <code>POINT_OUT</code>

To visualize results in 2D, open `ex_hdr.pvd` in ParaView which will automatically load the VTU files. You can select `PRESSURE1`, `TEMPERATURE1`, or `ELEMENT_VELOCITY` from a list of data arrays being plotted (e.g. Fig. 4 in the case of `PRESSURE1`). For details of how to use ParaView, please take a look the ParaView documentation (<http://www.paraview.org/paraview-guide/>).

Tips

- To plot the fluid velocity, it is recommended to use log scale since the velocities in the fracture and the matrix have different orders of magnitudes.
- To see a profile along the fracture, you can use *PlotOverLine* filter in ParaView. For example, Fig. 5 shows pressure and fluid velocity in the fracture using the filter.

The two CSV files, `ex_hdr_time_POINT_IN.csv` and `ex_hdr_time_POINT_OUT.csv`, contain simulated results at every time step at the inject and production wells. The results can easily be visualized, for example, using a spreadsheet software.

Results

Temperature distribution in the reservoir after 30 years of the water circulation is shown in Fig. 6. As one can expect, the reservoir gets colder near

the injection point and along the fracture toward the production point. Heat conduction process takes place in the low-permeable matrix near the injection point, while advective heat transport process is dominant in the fracture. Under the given conditions, the production temperature declines to about 175 °C (12.5% of the initial temperature(Fig. 7) after 30 years.

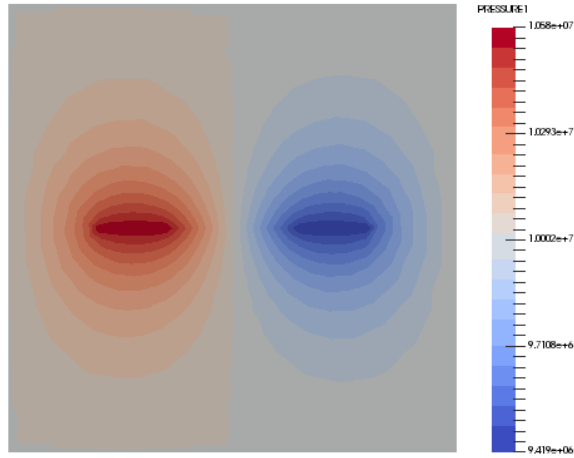


Fig. 4: Simulated steady-state pressure distribution visualized using ParaView

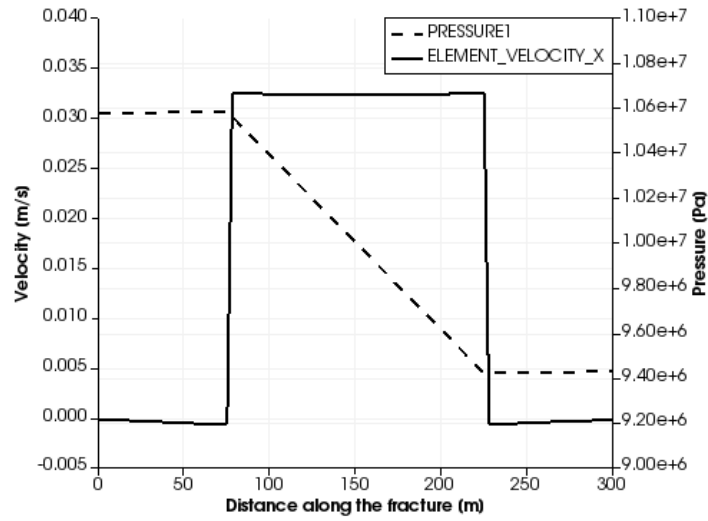


Fig. 5: Simulated fluid velocity and pressure along the fracture visualized using PlotOverLine filter in ParaView

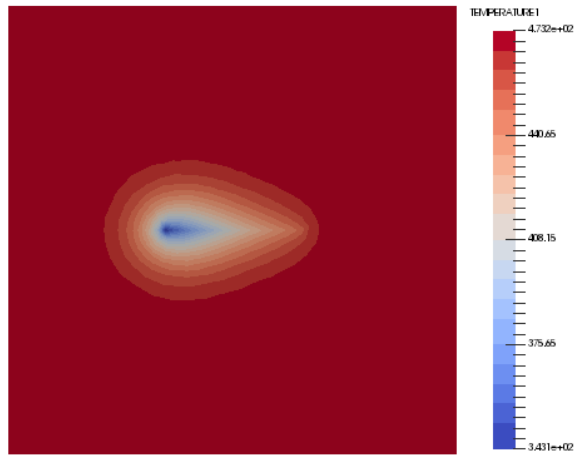


Fig. 6: Simulated temperature distribution after 30 years visualized using ParaView

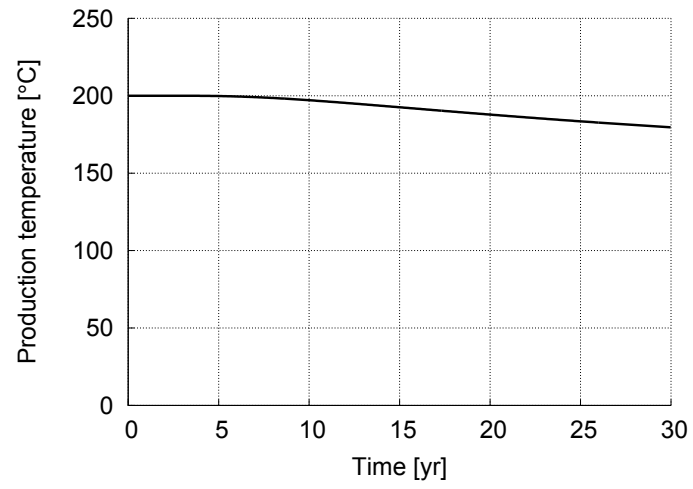


Fig. 7: Simulated temporal evolution of production temperature

4.2 2D Hot Sedimentary Aquifer benchmark

Problem Definition

The second example simulates heat extraction from a hot sedimentary aquifer where the formation fluid temperature reaches 150 °C (Fig. 8). Here sandstone is assumed as the rock type in the aquifer, which has a porosity of 10% and permeability of 10^{-15} m². A wellbore-doublet system is installed in the reservoir. The wellbores are separated by a distance of 200 m. A hydraulic fracture with a half length of 50 m is created from each wellbore for improving the reservoir transmissivity.

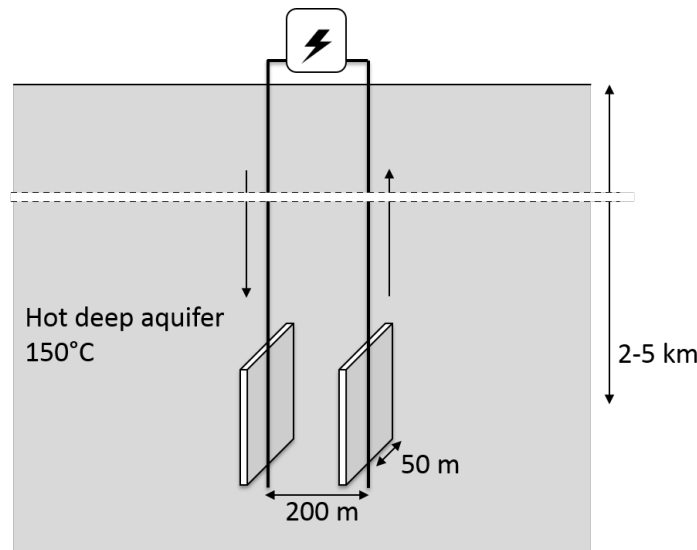


Fig. 8: Benchmark 2: Concept

The reservoir geometry can be simplified to a horizontal 2D model as shown in Fig. 9. We consider a scenario of circulating water at a rate of 3 L/s. The injected water has temperature of 70°C. Properties of the rock matrix, the fractures, and fluids are listed in Table 2. Same as the first example, temperature dependency on material properties is neglected except for the fluid viscosity.

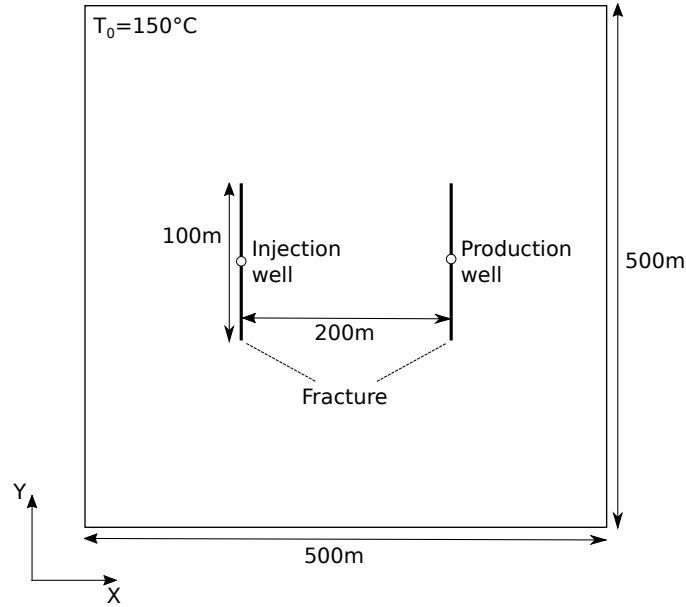


Fig. 9: Benchmark 2: Geometric layout

Property	Value
Initial reservoir temperature	150 °C
Initial reservoir pore pressure	10 MPa
Production rate	3 L/s
Injection rate	3 L/s
Injection temperature	70 °C
Fracture horizontal length	100 m
Fracture vertical length	100 m
Fracture mean aperture	100 μm
Fracture permeability	$8.3333 \cdot 10^{-10} \text{ m}^2$
Fracture porosity	100 %
Fracture storage	$4 \cdot 10^{-10} \text{ Pa}^{-1}$
Distance between the wells	200 m
Rock permeability	10^{-15} m^2
Rock porosity	10 %
Rock density	2600 kg/m ³
Rock specific heat capacity	950 J/kg/K
Rock thermal conductivity	3.0 W/m/K
Rock storage	10^{-10} Pa^{-1}
Fluid density	1000 kg/m ³
Fluid viscosity	Ramey et al (1974)
Fluid specific heat capacity	4200 J/kg/K
Fluid thermal conductivity	0.65 W/m/K

Table 2: Benchmark 2: Parameters

OGS Input Files

Input files for the second example is quite similar to those for the first example, except for the additional fracture and a mesh file. We explain only the following input files which are different from the first example:

- GLI
- MSH
- ST
- MSP
- MMP

Input files for the benchmark are available from <https://docs.opengeosys.org/books/geoenergy-modeling-iii>.

GLI - geometry

The following geometric objects are needed in this example for assigning boundary conditions and result outputs.

Listing 4.14: GLI input file

```
#POINTS
0 0 0 0
1 500 0 0
2 500 500 0
3 0 500 0
4 150 250 0 $NAME POINT_IN
5 350 250 0 $NAME POINT_OUT
#POLYLINE
$NAME
PLY_OUTER
$POINTS
0
1
2
3
0
#STOP
```

MSH - finite element mesh

Gmsh is again used for generating a mesh for this example. The matrix (material ID 0) and the fractures (material ID 1 and 2) are discretized with 2D triangular elements and 1D line elements, respectively. The following Gmsh input file describes the model geometry as well as the material grouping.

Listing 4.15: Gmsh input file

```

Mesh.Algorithm = 1;
Mesh.Optimize = 1;
lc=25;
lc2=2.5;
lc3=15;
Point(0)={0,0,0,lc};
Point(1)={500,0,0,lc};
Point(2)={500,500,0,lc};
Point(3)={0,500,0,lc};
Point(4)={150,200,0,lc2};
Point(5)={150,300,0,lc2};
Point(6)={350,200,0,lc2};
Point(7)={350,300,0,lc2};
Point(8)={150,250,0,lc2};
Point(9)={350,250,0,lc2};
Point(10)={250,250,0,lc3};
Line(1) = {0,1};
Line(2) = {1,2};
Line(3) = {2,3};
Line(4) = {3,0};
Line(5) = {4,8};
Line(6) = {8,5};
Line(7) = {6,9};
Line(8) = {9,7};
Line Loop(1) = {1,2,3,4};
Ruled Surface(1) = {1};
Line {5} In Surface {1};
Line {6} In Surface {1};
Line {7} In Surface {1};
Line {8} In Surface {1};
Point {10} In Surface {1};
Physical Surface(1) = {1};
Physical Line(2) = {5, 6};
Physical Line(3) = {7, 8};

```

After preparing the text file, run the following commands to execute Gmsh and convert a created Gmsh mesh file to an OGS mesh file. The generated mesh is shown in Fig. 10.

```

> gmsh ex_hsa.geo -2 -o ex_hsa.gmsh.msh
> GMSH2OGS -i ex_hsa.gmsh.msh -o ex_hsa.msh

```

ST - source/sink terms

The following example imposes an injection rate of 3 L/s ($3 \cdot 10^{-3} \text{ m}^3/\text{s}$) in the liquid flow process for the primary variable pressure at the point named POINT_IN and a production rate of 3 L/s at the point named POINT_OUT.

Listing 4.16: ST input file

```

#SOURCE_TERM
$PCS_TYPE
  LIQUID_FLOW
$PRIMARY_VARIABLE
  PRESSURE1
$GEO_TYPE
  POINT POINT_IN
$DIS_TYPE

```

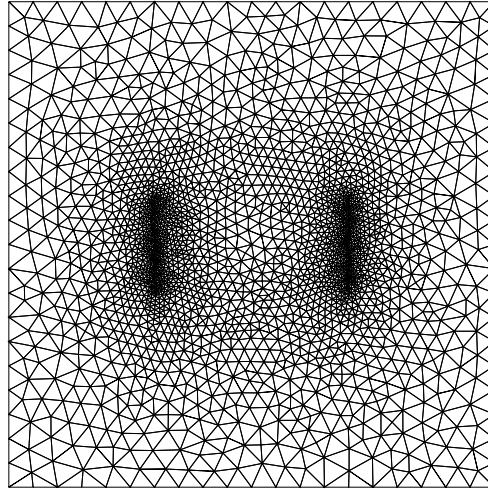


Fig. 10: Benchmark 2: An example mesh created by Gmsh

```

CONSTANT 3e-3 // unit m3/s
#SOURCE_TERM
$PCS_TYPE
LIQUID_FLOW
$PRIMARY_VARIABLE
PRESSURE1
$GEO_TYPE
POINT POINT_OUT
$DIS_TYPE
CONSTANT -3e-3
#STOP

```

MSP - solid properties

The next set of two files (MSP and MMP) are specifying material properties of solid phase and medium. In this second example, one needs to add one more definition because of the second fracture (material ID 2). Since the solid properties are same as the previous example, we can simply copy a definition of the first fracture to the second fracture.

Listing 4.17: MSP input file

```

; matrix
#SOLID_PROPERTIES
$DENSITY
1 2600
$THERMAL

```

```

EXPANSION
1e-005
CAPACITY
1 950
CONDUCTIVITY
1 3.0

; fracture 1
#SOLID_PROPERTIES
$DENSITY
1 2600
$THERMAL
EXPANSION
1e-005
CAPACITY
1 950.0
CONDUCTIVITY
1 3.0

; fracture 2
#SOLID_PROPERTIES
$DENSITY
1 2600
$THERMAL
EXPANSION
1e-005
CAPACITY
1 950.0
CONDUCTIVITY
1 3.0
#STOP

```

MMP - porous medium properties

Same as the MSP file, the MMP file should include a definition of the second fracture. In addition, some of the medium properties (i.e. the geometry area, the porosity, and the permeability) have to be changed since they are different from the first example (see Table 2).

Listing 4.18: MMP input file

```

; matrix
#MEDIUM_PROPERTIES
$GEOMETRY_DIMENSION
2
$GEOMETRY_AREA
100 // unit m
$POROSITY
1 0.10
$PERMEABILITY_TENSOR
ISOTROPIC 1e-15
$STORAGE
1 1e-10

; fracture 1
#MEDIUM_PROPERTIES
$GEOMETRY_DIMENSION
1
$GEOMETRY_AREA
1e-2 ; aperture 100 micro m

```

```
$POROSITY
1 1.0
$PERMEABILITY_TENSOR
ISOTROPIC 8.3333e-10
$STORAGE
1 4e-10

; fracture 2
#MEDIUM_PROPERTIES
$GEOMETRY_DIMENSION
1
$GEOMETRY_AREA
1e-2 ; aperture 100 micro m
$POROSITY
1 1.0
$PERMEABILITY_TENSOR
ISOTROPIC 8.3333e-10
$STORAGE
1 4e-10
#STOP
```

Results

Simulated steady-state pressure distribution and fluid velocity distribution are shown in Fig. 11 and Fig. 12. In contrast to the first example, water circulation can occur not only in the fractures but also in the rock matrix having some permeability. Temperature distribution after 30 years of the operation is shown in Fig. 13. Because of the combined conductive and advective heat transport, the larger volume of the reservoir is used for heat extraction. The produced temperature declines to 147.3 °C (1.8% reduction) after 30 years and to 128 °C (15% reduction) after 60 years (Fig. 14).

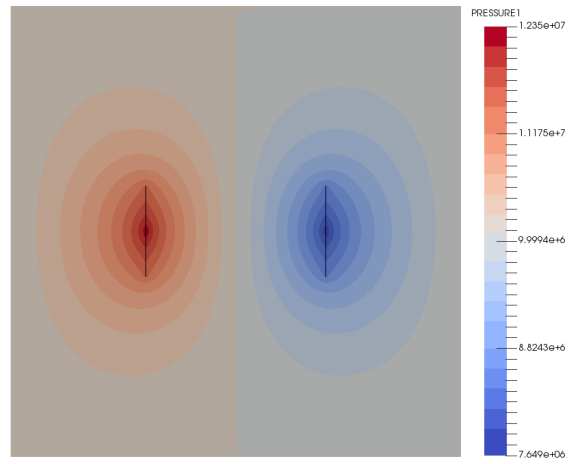


Fig. 11: Simulated steady-state pressure distribution

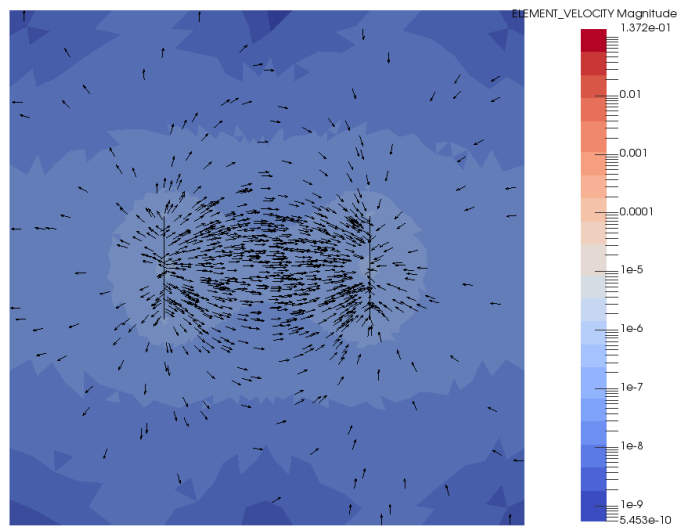


Fig. 12: Simulated fluid velocity distribution

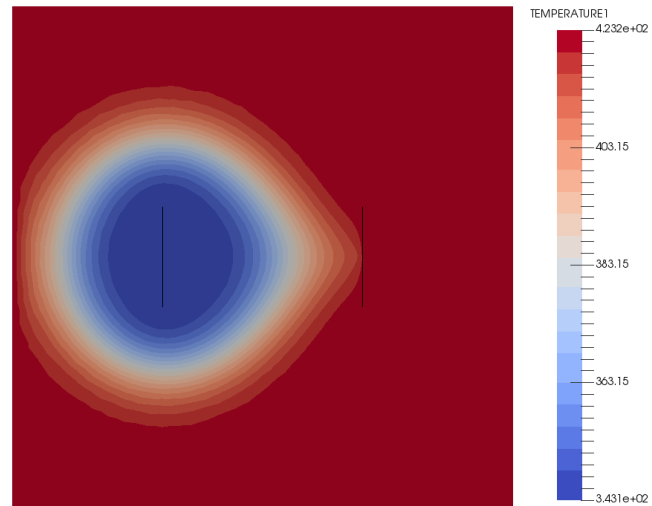


Fig. 13: Simulated temperature distribution after 30 years

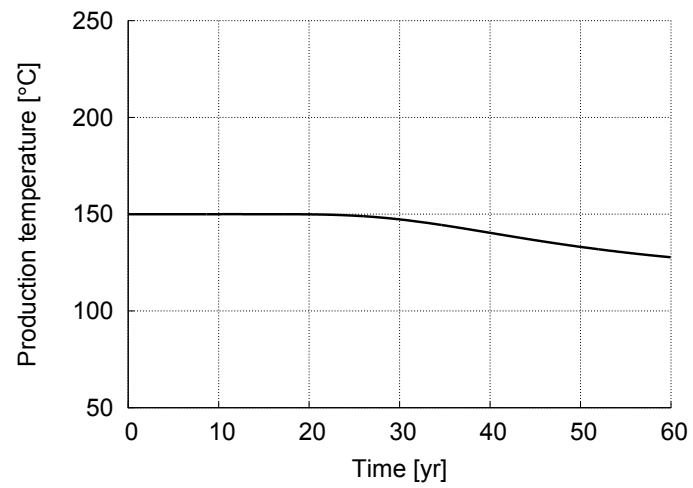


Fig. 14: Simulated production temperature over 60 years

Chapter 5

Case Study: Groß Schönebeck

In the following two chapters, we demonstrate how the numerical simulation can be applied to actual reservoir analysis. The first case study is given for the Groß Schönebeck research site in Germany, which represents a hot sedimentary aquifer type of EGS reservoirs. Input files for the simulations are available from <https://docs.opengeosys.org/books/geoenergy-modeling-iii>.

5.1 Site Description

The geothermal research site at Groß Schönebeck in the Northeast German Basin is located about 40 km north of Berlin, Germany (Fig. 1). The research site is one of the key in-situ laboratories in Germany for the investigation of an efficient provision of geothermal energy from deep sedimentary basins. The investigated geothermal reservoir of Groß Schönebeck is located between -3830 and -4250 m true vertical depth subsea (TVDSS). The faulted reservoir rocks can be roughly classified into siliciclastic sedimentary rocks consisting of conglomerates, sandstones and siltstones (Upper Rotliegend) and andesitic volcanic rocks (Lower Rotliegend). The siliciclastic rocks can be subdivided depending on their lithological properties into five formations (Blöcher et al, 2010). Of these five formations (Fig. 2), the Elbe base sandstones I and II are the most promising horizons for geothermal exploitation. They are characterized by a total thickness of approximately 100 m (-4000 to -4100 m TVDSS), a permeability locally higher than 1 mD (Trautwein and Huenges, 2005), a porosity of up to 10% (Huenges and Hurter, 2002), and a temperature of about 150°C (Wolfgramm et al, 2003). Hydraulic and thermal properties of all units and faults (Table 1 and Table 2) are based on previously published data (see Blöcher et al (2010) and references therein).

³ Reprinted from *Geothermics*, Vol. 39(1), Zimmermann G, Moeck I, Blöcher G, Cyclic waterfrac stimulation to develop an Enhanced Geothermal System (EGS) –

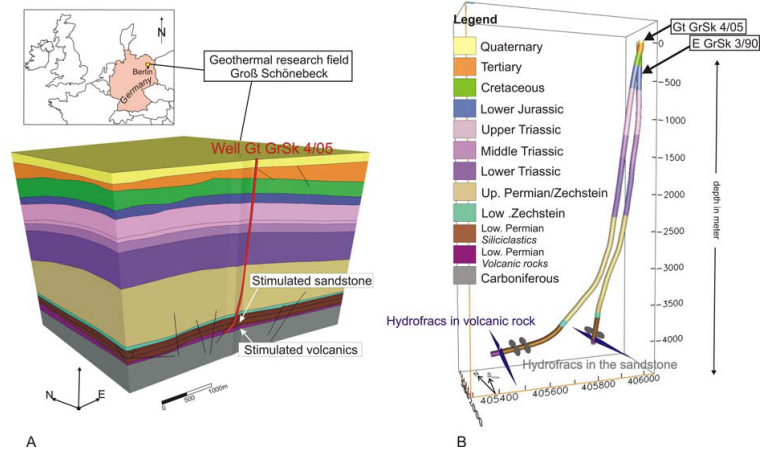


Fig. 1: (A) Location of the research drill site and 3D view of the geological horizons. The reservoir is situated in the Lower Permian within a depth of -3850 and -4258 m. (B) The two research wells with schematic illustration of hydraulically-induced fractures (Zimmermann et al, 2010) ³

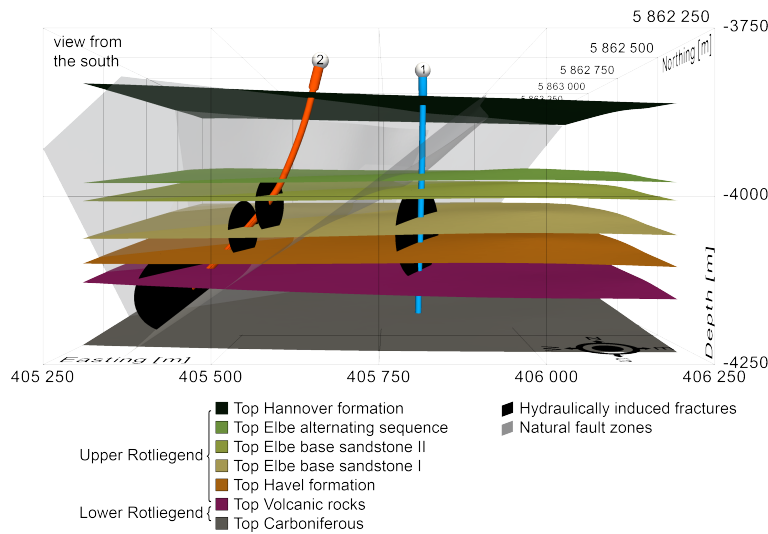


Fig. 2: Geological model developed on the basis of two-dimensional seismic and wellbore data. The injection well E GrSk 3/90 (1) is almost vertical and the production well Gt GrSk 4/05 A-2 (2) is directed towards a NE-striking/W-dipping fault. The black ellipses show the induced fractures of the doublet system at the Groß Schönebeck site (Blöcher et al, 2015) ⁴

Unit	Porosity [%]	Permeability [m ²]	Specific heat [J/kg/K]	Thermal conductivity [W/m/K]
Hannover formation	1	4.9E-17	920	1.9
Elbe alternating sequence	3	3.2E-16	920	1.9
Elbe base sandstone II	8	6.4E-16	920	3.1
Elbe base sandstone I	15	1.3E-15	920	3.2
Havel formation	0.1	9.9E-17	1000	3.0
Volcanic rocks	0.5	9.9E-17	1380	2.3

Table 1: Geological unit properties

Fault	Porosity [%]	Permeability [m ²]	Aperture [m]
Major fault zones	100	1.0E-15	1.0E-4
Minor fault zones	100	1.0E-13	1.0E-2
Induced fractures	100	1.0E-10	1.0E-2

Table 2: Fault/fracture properties

The sub-horizontal reservoir rocks are cross-cut by several natural fault zones striking preferentially from 130° (major faults) to 30° and 170° (minor faults) (Moeck et al, 2009). Within the current stress field, the latter bear the highest ratio of shear to normal stress, and are in a critically stressed state within the sandstones and in a highly stressed state within the volcanic layer (Fig. 3). According to previous studies which indicate a structural relationship between potential fluid flow along and across faults and their state of stress (Barton et al, 1995; Ito and Zoback, 2000), minor faults in Groß Schönebeck are assumed to be hydraulically transmissive, and the major fault zones are expected to behave as hydraulic barriers (Fig. 3).

Circulation of geothermal water is maintained via a thermal water loop consisting of a well doublet system with an injection (E GrSk 3/90) and a production (Gt GrSk 4/05 A-2) well, which was completed in 2007 (Fig. 2). The geothermal water loop was established in 2011 by additional surface flow lines (Frick et al, 2011). The injection well is an abandoned gas exploration

Conceptual design and experimental results, pp. 59–69, Copyright (2010), with permission from Elsevier.

⁴ Reprinted from *Computers & Geosciences*, Vol. 82, Blöcher G, Cacace M, Reinsch T, Watanabe N, Evaluation of three exploitation concepts for a deep geothermal system in the North German Basin, pp. 120–129, Copyright (2015), with permission from Elsevier.

⁵ Reprinted from *Computers & Geosciences*, Vol. 82, Blöcher G, Cacace M, Reinsch T, Watanabe N, Evaluation of three exploitation concepts for a deep geothermal system in the North German Basin, pp. 120–129, Copyright (2015), with permission from Elsevier.

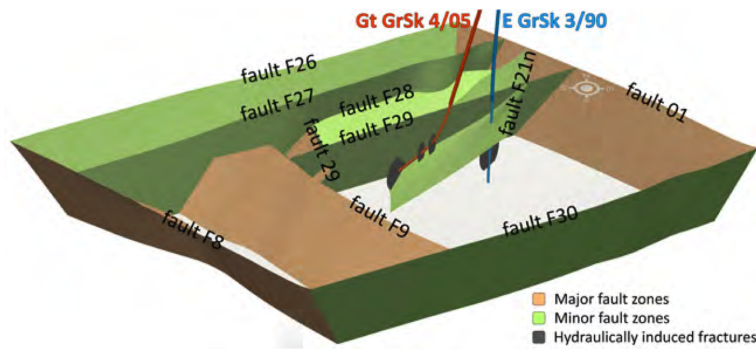


Fig. 3: Fault system of the Groß Schönebeck reservoir consisting of 130° striking major faults (hydraulic barriers), and 30° and 170° striking minor faults (hydraulically transmissive) (Blöcher et al, 2015) ⁵

well, which was reopened in 2001. The injection/production potential of the well was tested along the entire open hole section between -3799 m to -4228 m TVDSS. The production well Gt GrSk 4/05 A-2 was drilled along the minimal principal stress direction ($S_h = 288^\circ$ azimuth) with an inclination of up to 49° (Zimmermann et al, 2010) and a total depth of 4404.4 m MD. Due to the inclination the horizontal distance of both wells is ranging between 300 and 450 m in the reservoir section. In such a doublet configuration, it is the rock matrix that is the heat exchanger, a system that we call matrix-dominated.

To increase the efficiency of the doublet system three stimulation treatments and eight perforation treatments were performed in the production well and four stimulation treatments were performed in the injection well, which is cased with a perforated liner within the reservoir (Fig. 2). At the production well, a water-frac treatment was applied in the low permeability volcanic rocks and two gel-proppant treatments were used to stimulate the sandstone sections (Zimmermann and Reinicke, 2010; Zimmermann et al, 2010). At the injection well, two gel-proppant fracs and two water-fracs were performed within the same reservoir section and are henceforth referred to as "multi-frac" (Zimmermann et al, 2009). Since all induced fractures are mainly tensile, they are parallel to the maximum horizontal stress direction $\sigma_H = 18.5 \pm 3.7^\circ$ (Kwiątek et al, 2010). The geometry of the individual fractures is summarised in Table 3. The horizontal distance between the water-frac, first gel-proppant frac and second gel-proppant frac within the production well and the multi-frac within the injection well is 448, 352, and 308 m, respectively (Blöcher et al, 2010). The hydraulic and geometric properties (Table 2) of the induced fractures are estimated using modeled data based on measured field data (Zimmermann and Reinicke, 2010).

Frac type	Half-length [m]	Height [m]
Water-frac	190	175
Gel-proppant frac	60	95
Multi-frac	190	175

Table 3: Induced fracture geometric properties

5.2 Model Setup

This section explains numerical model setup for the Groß Schönebeck reservoir. In this tutorial, we simplify the reservoir structure and consider only major features so that one can execute simulations without cluster machines. The model takes into account a spatial domain with a horizontal extension of 3 x 3 km and a vertical extension of 0.6 km. The hydraulic fractures are located at the center of the domain. For reservoir structures, we take into account six geological formations, the conductive fault zone F21n locating in between the two wells, four hydraulic fractures, an open-hole section of the production well, and an intersection point of the injection well with multi-frac where we assume fluid flows into the reservoir. In addition, we include one buffer layer below the bottom geological unit to avoid an influence of boundary conditions. The additional layer has the same properties as the volcanic rocks. For each component of the model, we assign distinct material IDs to specify their properties (Fig. 4).

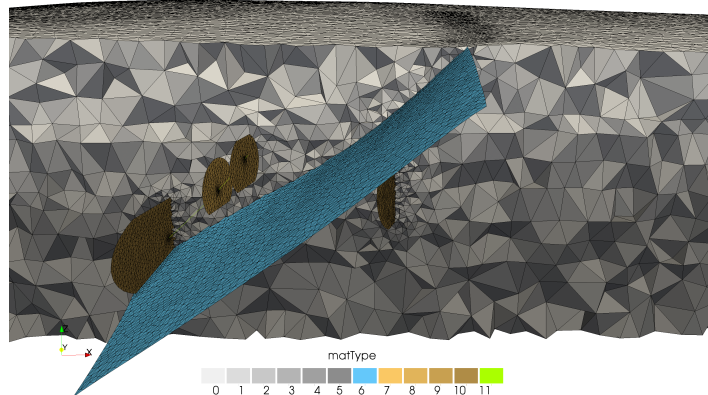


Fig. 4: A finite element mesh of the simplified 3D geological model with material group assignments

To consider influences of varying fluid density and viscosity, fluid density is related to temperature T , pressure p and salinity concentration C :

$$\rho = \rho_0 + \beta(T - T_0) + \gamma(p - p_0) + \alpha(C - C_0)$$

with linear coefficients β for temperature, γ for pressure, and α for concentration (Magri et al, 2005). In this study, we set $\rho_0 = 1081.25$, $\beta = -0.2259$, $T_0 = 348.15$, $\gamma = 4.442e-7$, $p_0 = 1E5$, $\alpha = 563.89E-3$, $C = 265$, and $C_0 = 150$. The dynamic viscosity of the fluid is regarded as a function of salinity concentration and temperature (Diersch, 2002), expressed with the mass fraction ω and relative temperature coefficient ζ :

$$\frac{\mu_0}{\mu} = \frac{1 + 0.7063\zeta - 0.04832\zeta^3}{1 + 1.85\omega - 4.1\omega^2 + 44.5\omega^3}; \quad \omega = \frac{C}{\rho}; \quad \zeta = \frac{T - 150}{100}$$

with $\mu_0 = 0.001$, $C_0 = 0$, and $T_0 = 298.15$.

For in-situ pressure and temperature field, a hydrostatic boundary condition on each of the four vertical borders is applied with an assumption of a fluid density of 1148 kg/m^3 . Furthermore, a temperature gradient of $28 \text{ }^\circ\text{C/km}$ is applied to computing temperature on the top surface. To simulate the terrestrial heat flux, we set a value of 72 mW/m^2 at the bottom surface. Initial pressure and temperature in the reservoir are obtained by a steady-state simulation with the given boundary conditions.

For the reservoir simulation with heat extraction, an injection rate of $30 \text{ m}^3/\text{h}$ is applied at the center of the hydraulic induced fracture at the injection well. The production rate of $30 \text{ m}^3/\text{h}$ is applied at the top of the well section of the production site. Alternation of all properties regarding the geological units, hydraulic induced fractures and fault zones is not considered. To simulate the life cycle performance of the geothermal doublet system, a minimum simulation time of 30 years is required.

5.3 Mesh Generation

This section explains how to generate a finite element mesh for the Groß Schönebeck reservoir model using MeshIt (Cacace and Blöcher, 2015). Before starting the mesh generation, please make sure that you have the following input files from <https://docs.opengeosys.org/books/geoenergy-modeling-iii>.

Directory	File name
grsk/mesh/input/wells	GtGrSk405.csv EGrSk390.csv
grsk/mesh/input/faults	F21n.csv
grsk/mesh/input/fractures	01_water_elip.csv 02_1st_gel_elip.csv 03_2nd_gel_elip.csv 04_multi_elip.csv
grsk/mesh/input/units	01_top_hannover.csv 02_top_dethlingen.csv 03_top_ebs.csv 04_top_rockel.csv 05_top_havel.csv 06_top_vulkanit.csv 07_top_karbon.csv 08_bottom.csv
grsk/mesh/input/border	border1.csv border2.csv border3.csv border4.csv

Importing geometry data

The first step is to import all the geometry data into MeshIt (Fig. 5).

1. Open MeshIt and import the wells EGrSk390.csv and GtGrSk405.csv by "File → Add → Well...".
2. Import all the border files by "File → Add → Border...".
3. Import the fault F21n.csv and all the fractures by "File → Add → Faults...".
4. Import all the units by "File → Add → Unit...".

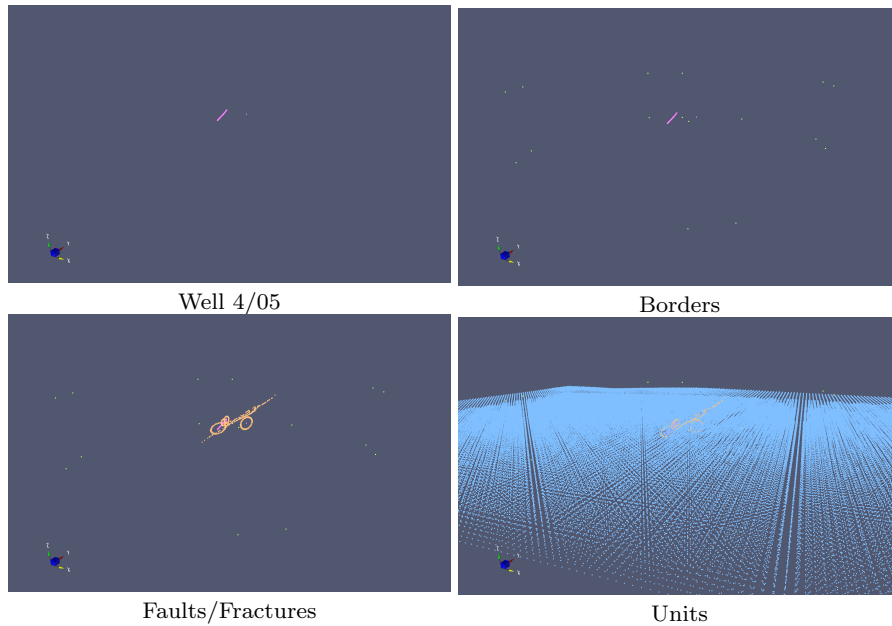


Fig. 5: Imported geometry in MeshIT

Surface meshing

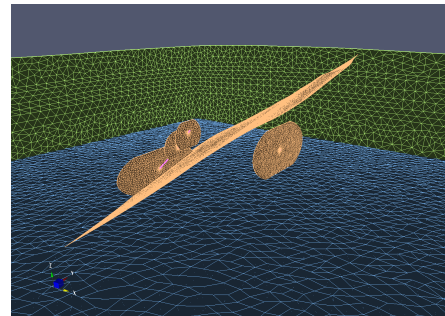
After importing all the geometry, a surface mesh has to be constructed before creating a 3D mesh. Go to the refinement menu "Edit → Refinement..." and insert the following refinements for each component (Fig. 6):

1. Borders and Units: 60 m; Faults: 20 m; induced Fractures: 10 m; Wells: 2 m

2. In the mesh quality dialog the interpolation algorithm “Kriging” should be selected for the triangle generation.
3. Click ”preMesh”
4. “Save”

Object	Refinement
01_top_han...	60
02_top_det...	60
03_top_ebs	60
04_top_roc...	60
05_top_havel	60
06_top_vul...	60
07_top_kar...	60
08_bottom	60
F21n	20
1st_gel_elip	10
2nd_gel_elip	10
multi_elip	10
water_elip	10
border1	60
border2	60
border3	60
border4	60
EGrSk390	2
GtGrSk405	2

Triangle menu



Generated surface mesh

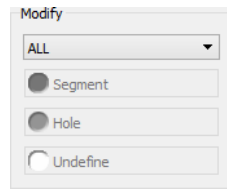
Fig. 6: Surface meshing

Selecting constrains of the final mesh

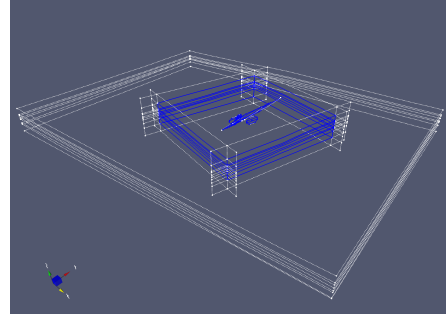
The next step is to select constrains which you want to include in the final mesh (Fig. 7).

1. Uncheck all views
2. Select “All” in the Modify menu
3. In the drop down menu, you can select the surface of interest. You can now define the intersection as a “Segment” or “Hole” in the final volume mesh.
4. Select `01_top_hannover` in the drop down menu, and click segments as shown in Fig. 8. Selected segments are colored with blue.

5. Follow the same for all the other units (Fig. 8), faults (Fig. 9), fractures (Fig. 10), borders (Fig. 11) and wells (Fig. 12).



Modify menu



View

Fig. 7: Selecting constraints of the final mesh

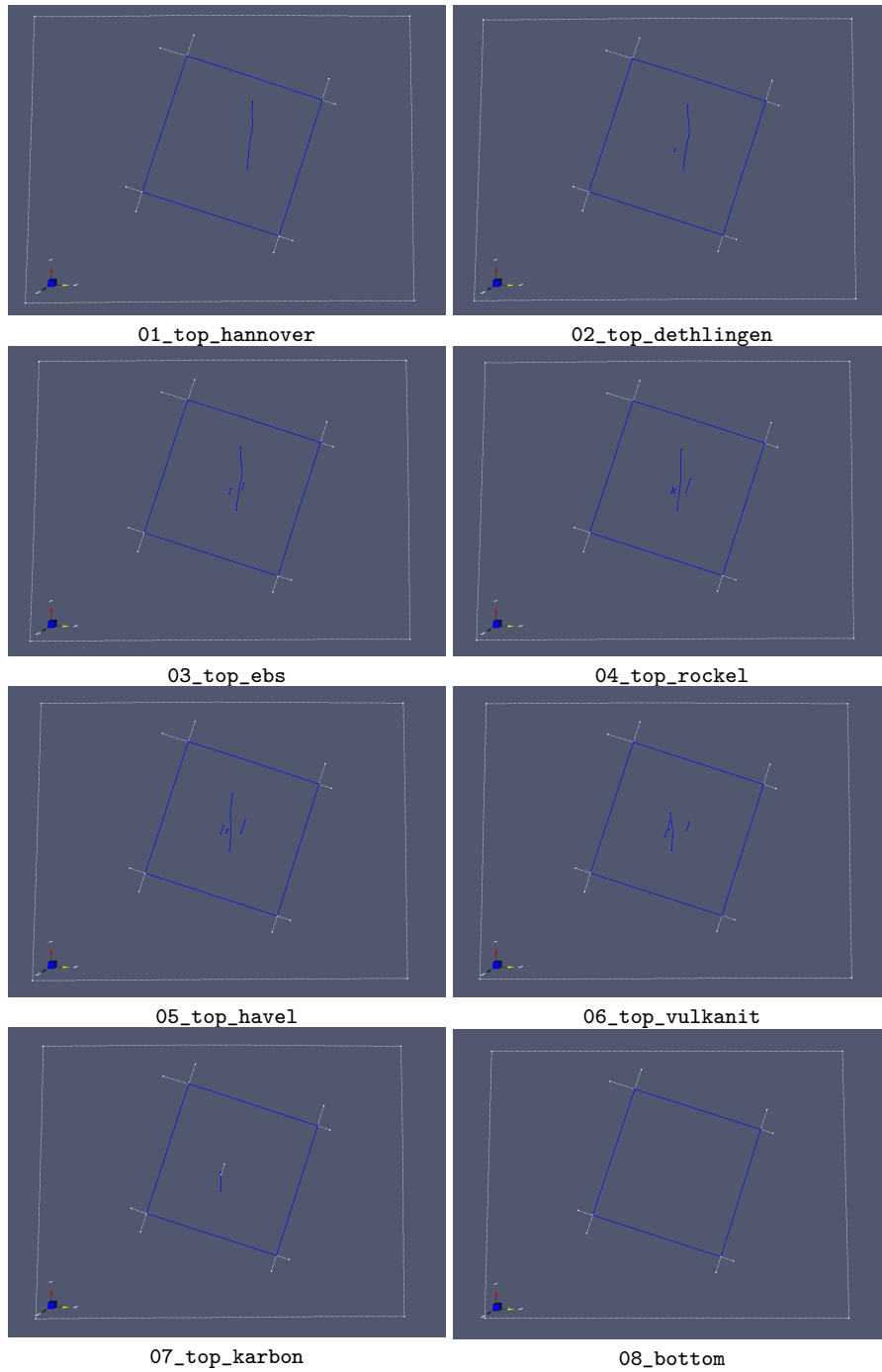
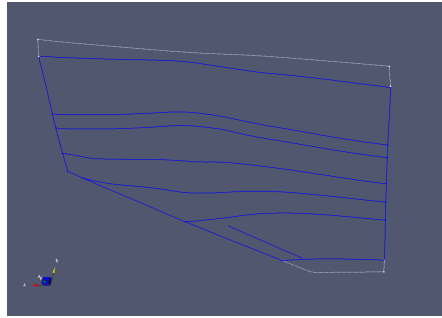
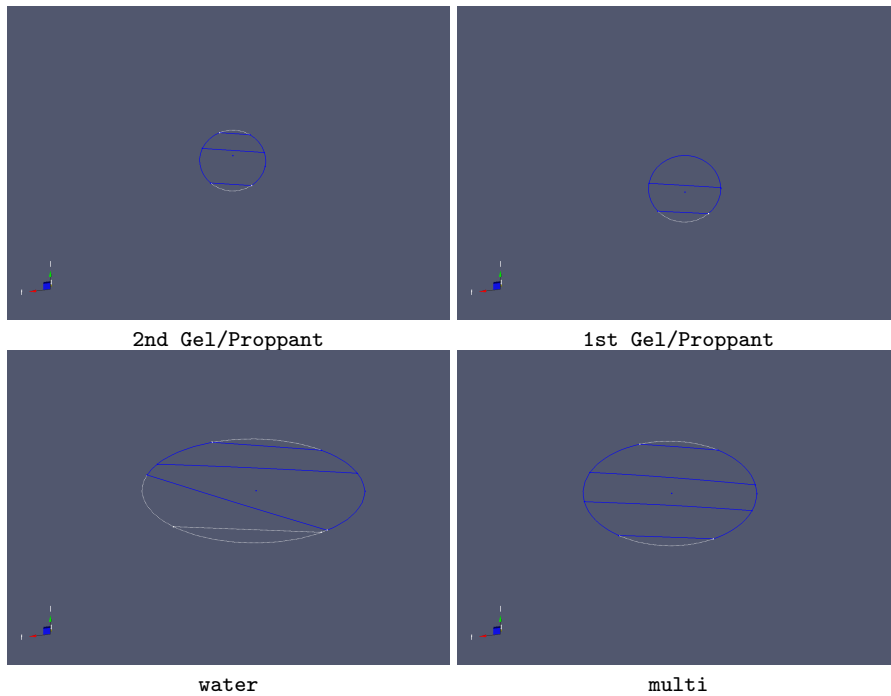


Fig. 8: Selecting constraints for units



F21n

Fig. 9: Selecting constraints for fault



2nd Gel/Proppant

1st Gel/Proppant

water

multi

Fig. 10: Selecting constraints for fractures

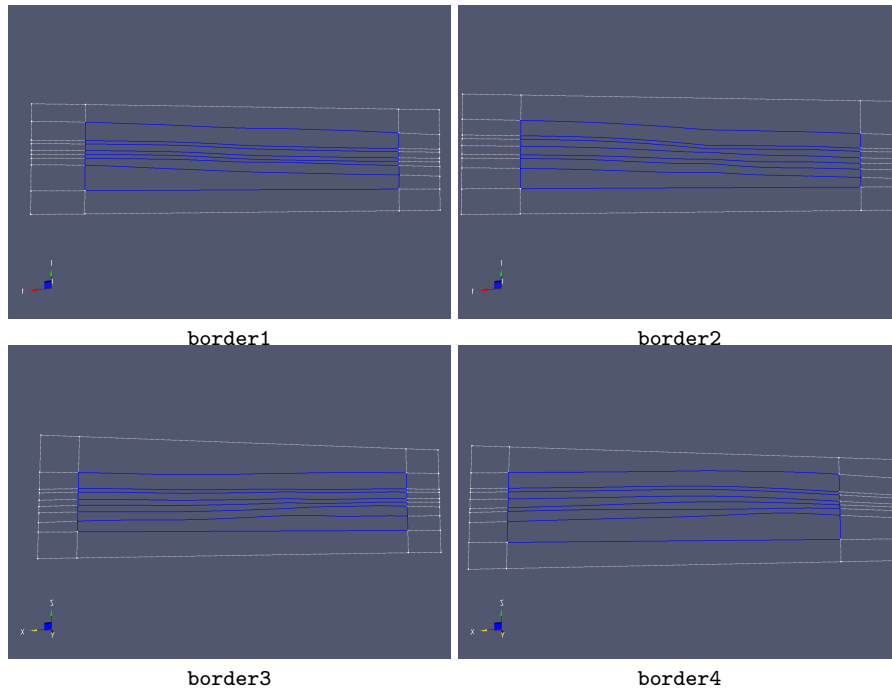


Fig. 11: Selecting constraints for borders

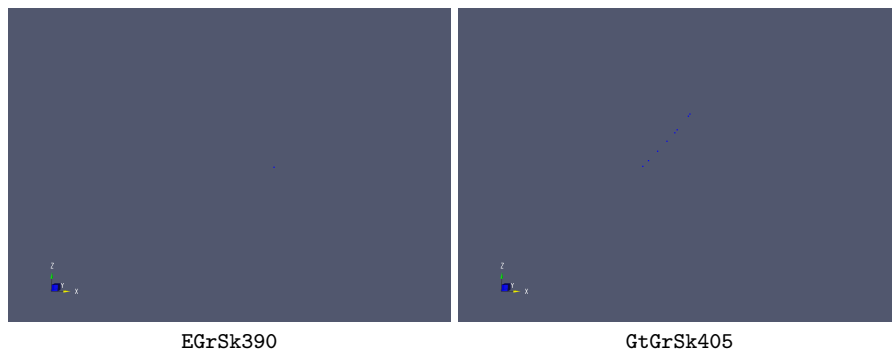


Fig. 12: Selecting constraints for well

Assigning 3D Materials

The last step before generating a 3D mesh is assigning material IDs for each component being included in the mesh (Fig. 13).

1. Select “OFF” from the “MODIFY” menu
2. Turn on “Surface Faces” and “Intersection Edges” for each Unit
3. Assign 1D MaterialIDs for Well 405
4. Assign 2D MaterialIDs for each fault and fracture
5. Assign 3D MaterialIDs for each sub domain of units

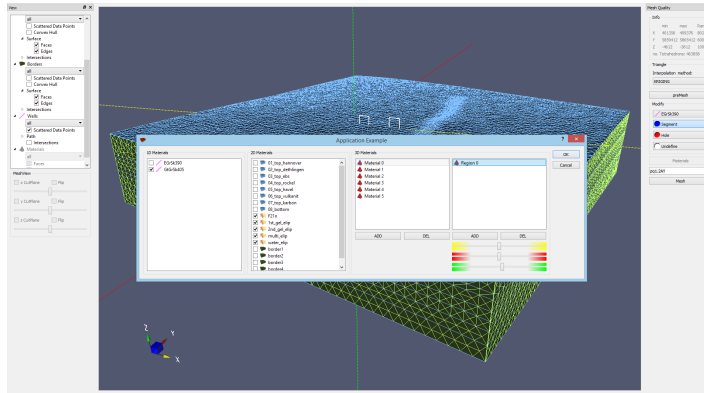


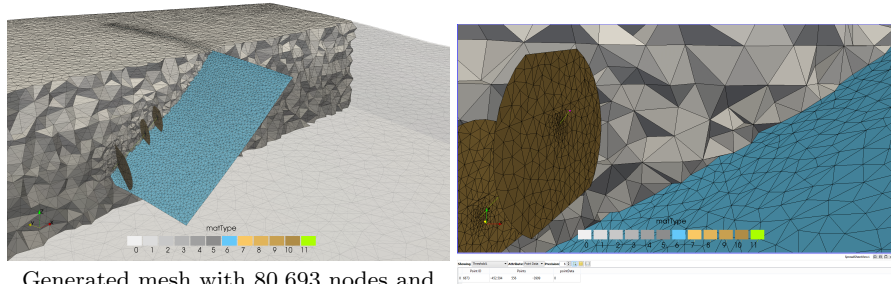
Fig. 13: Assigning Material IDs

Volume Meshing and Exporting

Now you are ready to generate a final 3D mesh. After the mesh generation, a resulted 3D mesh and surface meshes have to be exported for visualizations and numerical simulations.

1. Click “Mesh” in the right panel. This may take some minutes. Save data afterwards.
2. For simulation, “Export” 3D mesh to OGS mesh format. Save a mesh in `grsbk.msh`.
3. “Export” all vertical borders as separate TIN files (pressure boundaries).
4. “Export” top and bottom surfaces as separate TIN files (temperature boundaries).
5. For visualization, “Export” 3D mesh to “ParaView” format. Save a mesh in `mesh.vtu`.

6. Open the exported `mesh.vtu` with ParaView. Select a point along the well and extract the coordinates.



Generated mesh with 80,693 nodes and 477,085 elements (146 lines, 13,081 triangles, 463,858 tetrahedron)

Select a point along the well

Fig. 14: Visualization of the generated mesh with ParaView

At the end, the following files should be generated.

- `grsbk.msh`
- `01_top_hannover.tin`
- `08_bottom.tin`
- `border1.tin`
- `border2.tin`

5.4 Simulation of Initial Reservoir Conditions

The next step after the mesh generation is to determine initial conditions, i.e. undisturbed state, of the reservoir. The initial conditions will be used as a starting point of simulating heat extraction process (section 5.5). We estimate the initial conditions by simulating a stationary state of pressure and temperature fields in the reservoir with natural boundary conditions (e.g. terrestrial heat flux) but without any fluid injection and production. The following subsections explain OGS input files for the steady state simulation and result examples.

5.4.1 Input Files

GLI - geometry

The GLI file should contain definitions of points and surfaces defining well-bore heads and outer domain surfaces. These geometric objects are used for boundary condition assignments. Complex surface geometries are specified using a TIN file with \$TIN keyword followed by a file name.

Listing 5.1: GLI input file

```
#POINTS
0 405825.6875 5862677.0 -4070.5 $NAME WELL_GrSk3
1 405547.4 5862555.8 -3999 $NAME WELL_GrSk4
#SURFACE
$NAME
top
$TIN
01TopHann.tin
#SURFACE
$NAME
bottom
$TIN
bottom.tin
#SURFACE
$NAME
border1
$TIN
border1.tin
#SURFACE
$NAME
border2
$TIN
border2.tin
#STOP
```

PCS - process definition

A steady-state simulation is specified in \$TIM_TYPE with STEADY keyword. The well elements (Material ID 12) has to be excluded from the steady state simulation by setting \$DEACTIVATED_SUBDOMAIN. To let OGS output restart files for another simulations, \$RELOAD keyword has to be provided with a mode 1 .

Listing 5.2: PCS input file

```
#PROCESS
$PCS_TYPE
  LIQUID_FLOW
$TIM_TYPE
  STEADY
$RELOAD
  1 1
$DEACTIVATED_SUBDOMAIN
  1
  12 ; well GrSk4
#PROCESS
$PCS_TYPE
  HEAT_TRANSPORT
$TIM_TYPE
  STEADY
$RELOAD
  1 1
$DEACTIVATED_SUBDOMAIN
  1
  12 ; well GrSk4
#STOP
```

NUM - numerical properties

The NUM file should be configured as shown in Listing 5.3. To suppress numerical oscillations in heat transport, the mass lumping technique \$ELE_MASS_LUMPING and the Streamline Upwind/Petrov-Galerkin (SUPG) method \$ELE_SUPG are enabled.

Listing 5.3: NUM input file

```
$OVERALL_COUPLING
;min_iter -- max_iter
  1          25
#NUMERICS
$PCS_TYPE
  LIQUID_FLOW
$LINEAR_SOLVER
;method error_tolerance max_iterations theta precondition storage
  4      6 1.e-012      3000          1.0  2          4
$EXTERNAL_SOLVER_OPTION
  -ilu_fill 1
$NON_LINEAR_ITERATIONS
;type -- error_method -- max_iterations -- relaxation -- tolerance(s)
  PICARD LMAX 25 0.0 10
$COUPLING_CONTROL
```

```

;error method -- tolerances
LMAX 10
#NUMERICS
$PCS_TYPE
HEAT_TRANSPORT
$LINEAR_SOLVER
;method error_tolerance max_iterations theta precondition storage
9 6 1.e-012 3000 1.0 9 4
; 9 6 1.e-012 3000 1.0 9 4
$EXTERNAL_SOLVER_OPTION
-ilu_fill 1
$NON_LINEAR_ITERATIONS
;type -- error_method -- max_iterations -- relaxation -- tolerance(s)
PICARD LMAX 25 0.0 1e-3
$COUPLING_CONTROL
;error method -- tolerances
LMAX 1.e-3
$ELE_MASS_LUMPING
1
$ELE_SUPG
1 0 0
#STOP

```

TIM - time discretization

For steady state, only one time step is required (nothing will change with time).

Listing 5.4: TIM input file

```

#TIME_STEPPING
$PCS_TYPE
LIQUID_FLOW
$TIME_START
0
$TIME_END
1
$TIME_STEPS
1 1
#TIME_STEPPING
$PCS_TYPE
HEAT_TRANSPORT
$TIME_START
0
$TIME_END
1
$TIME_STEPS
1 1
#STOP

```

IC - initial conditions

Although no initial conditions are required for steady state simulations, we provide the best guess, i.e. depth-dependent linear distributions assuming a

fluid density of 1148 kg/m^3 and a geothermal gradient of 0.028 K/m . Distribution type `$GRADIENT` can be used for this purpose.

Listing 5.5: IC input file

```
#INITIAL_CONDITION
$PCS_TYPE
LIQUID_FLOW
$PRIMARY_VARIABLE
PRESSURE1
$GEO_TYPE
DOMAIN
$DIS_TYPE
GRADIENT -3760 3.68856e7 11261.88 ; rho_f = 1148
#INITIAL_CONDITION
$PCS_TYPE
HEAT_TRANSPORT
$PRIMARY_VARIABLE
TEMPERATURE1
$GEO_TYPE
DOMAIN
$DIS_TYPE
GRADIENT -3816 410.65 0.028
#STOP
```

BC - boundary conditions

In the BC input file, prescribed values have to be provided. In this example, we set hydrostatic pressure at lateral boundaries and prescribed temperature at the top surface. Both distributions are depth-dependent and therefore are given by using `$GRADIENT` keyword.

Listing 5.6: BC input file

```
#BOUNDARY_CONDITION
$PCS_TYPE
LIQUID_FLOW
$PRIMARY_VARIABLE
PRESSURE1
$GEO_TYPE
SURFACE border1
$DIS_TYPE
GRADIENT -135 100000 11261.88 ; rho_f = 1148
#BOUNDARY_CONDITION
$PCS_TYPE
LIQUID_FLOW
$PRIMARY_VARIABLE
PRESSURE1
$GEO_TYPE
SURFACE border2
$DIS_TYPE
GRADIENT -135 100000 11261.88 ; rho_f = 1148
#BOUNDARY_CONDITION
$PCS_TYPE
HEAT_TRANSPORT
$PRIMARY_VARIABLE
TEMPERATURE1
$GEO_TYPE
```

```

SURFACE top
$DIS_TYPE
GRADIENT -3816 410.65 0.028
#STOP

```

ST - source/sink terms

In the ST input file, source/sink terms and Neumann boundary conditions are specified. Here we set a terrestrial heat flux of 72 mW/m^2 through the bottom surface.

Listing 5.7: ST input file

```

#SOURCE_TERM
$PCS_TYPE
HEAT_TRANSPORT
$PRIMARY_VARIABLE
TEMPERATURE1
$GEO_TYPE
SURFACE bottom
$DIS_TYPE
CONSTANT_NEUMANN .072 ; 72 mW/m2
#STOP

```

MFP - fluid properties

The MFP input file defines fluid properties including the variable fluid density and viscosity models explained above. Specific heat and thermal conductivity are assumed as invariant.

Listing 5.8: MFP input file

```

#FLUID_PROPERTIES
$DENSITY
21 1081.25 1e+5 4.442e-7 150.0 563.89e-3 348.15 -0.2259 265
; 21 rho0 p0[Pa] rho0_p C0[g/L] rho0_c T0[K] rho0_T C[g/L]
$VISCOSITY
21 0.001 1e+5 0 298.15 -1 300
; 21 vis0 p0[Pa] C0[g/L] T0[K] rho0 C[g/L] T[K](optional)
$SPECIFIC_HEAT_CAPACITY
1 4193.5
$HEAT_CONDUCTIVITY
1 0.65
#STOP

```

MSP - solid properties

The MSP input file should contain solid phase definitions of the geological units, the faults, the fractures, and the well. Unit properties can be given according to Table 1. An example definition for the first geological unit is given below.

Listing 5.9: Matrix definition example in MSP input file

```
;0 Unit I - Silit and mudstone
#SOLID_PROPERTIES
$DENSITY
 1 2650
$THERMAL
EXPANSION 1.0e-5
CAPACITY:
 1 920
CONDUCTIVITY:
 1 1.91
$ELASTICITY
POISSON 0.2
YOUNGS_MODULUS:
 1 5.5e+10
```

Solid phase properties also have to be given for all the faults, fractures, and wells, even though they have only a fluid phase. We set some dummy values for them, which are not used in the simulation.

Listing 5.10: Fault/fracture definition example in MSP input file

```
;7 Fault F21n (conductive)
#SOLID_PROPERTIES
$DENSITY
 1 2650
$THERMAL
EXPANSION 1.0e-5
CAPACITY:
 1 1000
CONDUCTIVITY:
 1 3.0
$ELASTICITY
POISSON 0.2
YOUNGS_MODULUS:
 1 5.5e+10
```

MMP - porous medium properties

In the MMP input file, medium properties have to be provided according to Table 1 and Table 2. Example definitions for the unit, the fracture, and the well are shown below.

Listing 5.11: Matrix definition example in MMP input file

```
;0 Unit I - Silit and mudstone
```

```

#MEDIUM_PROPERTIES
$GEOMETRY_DIMENSION
3
$GEOMETRY_AREA
1.0
$POROSITY
1 0.01
$STORAGE
1 1e-10
$PERMEABILITY_TENSOR
ORTHOTROPIC 4.9346e-17 4.9346e-17 1.2336e-17

```

Listing 5.12: Fault/fracture definition example in MMP input file

```

;7 Fault F21n (conductive)
#MEDIUM_PROPERTIES
$GEOMETRY_DIMENSION
2
$GEOMETRY_AREA
1.00e-2
$POROSITY
1 1.0
$STORAGE
1 4e-10
$PERMEABILITY_TENSOR
ISOTROPIC 1.00e-13

```

Listing 5.13: Wellbore definition example in MMP input file

```

;12 production wellbore
#MEDIUM_PROPERTIES
$GEOMETRY_DIMENSION
1
$GEOMETRY_AREA
7.854e-3 ; r=5cm
$POROSITY
1 1.0
$STORAGE
1 4e-10
$PERMEABILITY_TENSOR
ISOTROPIC 1e-6

```

OUT - output parameters

In the OUT input file, we define three configurations: 1) output of results for the entire domain in PVD and VTU files, 2) output of time-series values at the injection point `WELL_GrSk3` in a CSV file, and 3) output of time-series values at the top of the production wellbore open-hole section `WELL_GrSk4` in a CSV file.

Listing 5.14: OUT input file

```

#OUTPUT
$NOD_VALUES

```

```

PRESSURE1
TEMPERATURE1
$ELE_VALUES
VELOCITY1_X
$MFP_VALUES
DENSITY
VISCOSITY
$GEO_TYPE
DOMAIN
$DAT_TYPE
PVD
$TIM_TYPE
STEPS 1
#OUTPUT
$NOD_VALUES
PRESSURE1
TEMPERATURE1
$GEO_TYPE
POINT WELL_GrSk3
$DAT_TYPE
CSV
$TIM_TYPE
STEPS 1
#OUTPUT
$NOD_VALUES
PRESSURE1
TEMPERATURE1
$GEO_TYPE
POINT WELL_GrSk4
$DAT_TYPE
CSV
$TIM_TYPE
STEPS 1
#STOP

```

5.4.2 Results

After executing OGS with the above input files, one should obtain PVD/VTU files and the following restart files which are used in the next transient simulation.

- grsk_LIQUID_FLOW_PRESSURE1_primary_value_1.asc.
- grsk_HEAT_TRANSPORT_TEMPERATURE1_primary_value_1.asc.

Simulated steady-state pressure and temperature fields can be visualized with ParaView as shown in Fig. 15 and Fig. 16. Using *PlotOverLine* filter, one can plot vertical profiles of pressure and temperature (see Fig. 17). As shown in the figure, the temperature distribution is not linearly dependent on the depth and is influenced by nonuniform fluid properties and geological units having different thermal properties. The simulated temperature profile is in good agreement with the measured data.

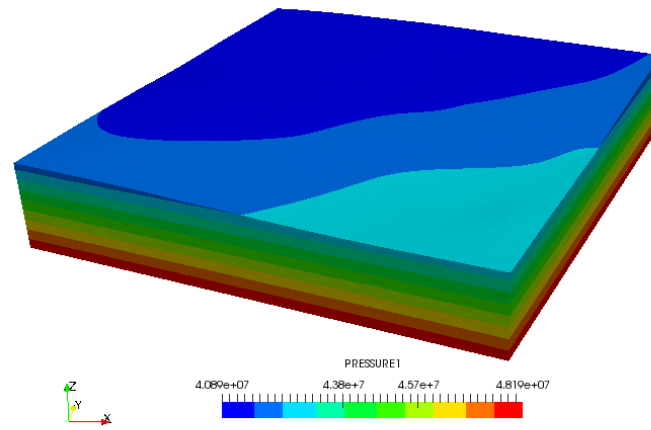


Fig. 15: Simulated steady-state pressure distribution

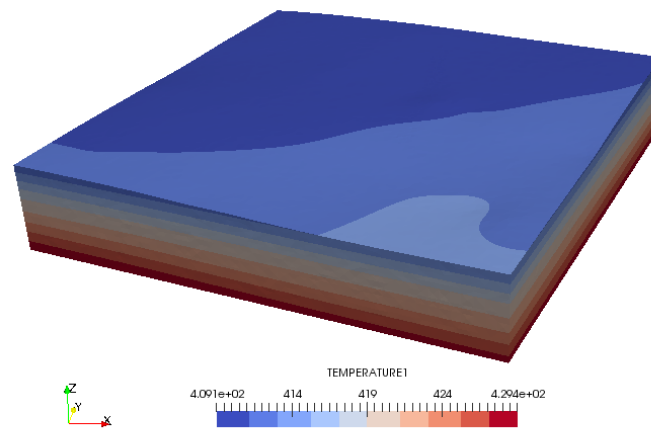


Fig. 16: Simulated steady-state temperature distribution

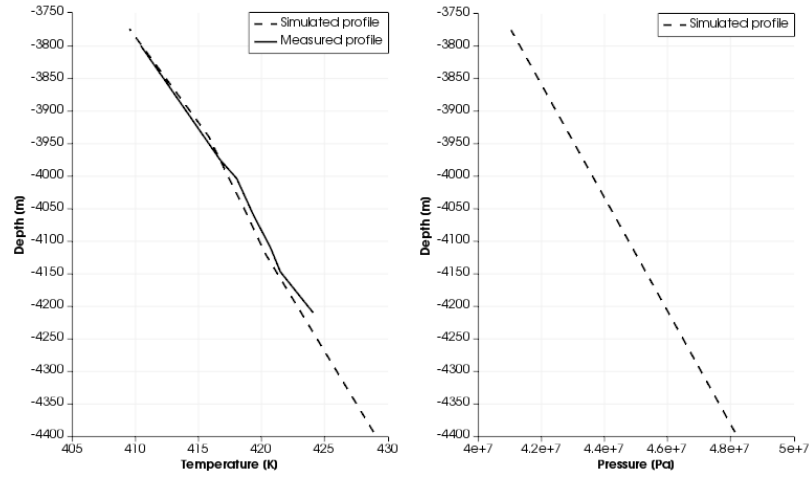


Fig. 17: Vertical profiles of simulated temperature and pressure using *PlotOverLine* filter

5.5 Simulation of Heat Extraction Process

This section explains transient simulation of heat extraction from the reservoir. As a preparation for the transient simulation, please copy the restart files generated in the previous simulation to the working directory for the transient simulation. To help OGS detect the restart files, please remove "_1" from the restart file names. Having the renamed restart files, we are ready to simulate thermal-hydraulic processes in the reservoir accompanied with heat extraction. The following subsections explain only the input files which are different from the steady-state simulation.

PCS - process definition

To use the restart files as initial conditions, `$RELOAD` has to be changed to mode 2.

Listing 5.15: PCS input file

```
#PROCESS
$PCS_TYPE
LIQUID_FLOW
$RELOAD
2 1
#PROCESS
$PCS_TYPE
HEAT_TRANSPORT
$RELOAD
2 1
#STOP
```

TIM - time discretization

For the transient case, we need maximum 30 years of simulation time. As the system behavior is highly dynamic at the beginning of the simulation, time stepping is started with a very small length and is gradually increased.

Listing 5.16: A part of TIM input file

```
#TIME_STEPPING
$PCS_TYPE
LIQUID_FLOW
$TIME_START
0
$TIME_END
1000000000
$TIME_STEPS
10 0.001
9 0.01
9 0.1
9 1
```

```

9 10
9 100
9 1000
9 10000
9 100000
9 1000000
99 10000000
#TIME_STEPPING

```

BC - boundary conditions

For the transient simulation, no temperature boundary condition at the top is required. Instead, temperature of 70°C is to be set at the injection well point.

Listing 5.17: Addition in the BC input file

```

#BOUNDARY_CONDITION
$PCS_TYPE
HEAT_TRANSPORT
$PRIMARY_VARIABLE
TEMPERATURE1
$GEO_TYPE
POINT WELL_GrSk3
$DIS_TYPE
CONSTANT 343.15

```

ST - source/sink terms

For the transient simulation, the injection and production rate (30 m³/h) must be implemented at points WELL_GrSk3 and WELL_GrSk4.

Listing 5.18: Addition in the ST input file

```

#SOURCE_TERM
$PCS_TYPE
LIQUID_FLOW
$PRIMARY_VARIABLE
PRESSURE1
$GEO_TYPE
POINT WELL_GrSk3
$DIS_TYPE
CONSTANT 0.008333333 ; 30m3/h
#SOURCE_TERM
$PCS_TYPE
LIQUID_FLOW
$PRIMARY_VARIABLE
PRESSURE1
$GEO_TYPE
POINT WELL_GrSk4
$DIS_TYPE
CONSTANT -0.008333333 ; -30m3/h

```

5.5.1 Results

After executing OGS with the above input files, one should obtain PVD/VTU files for distributed values and CSV files for time profiles at the injection and production points.

The temporal profiles of pressure show that, after nearly 30 years, pressure at the injection point increased up to 62 MPa (Fig. 18) and pressure at the top of the production well decreased to 34 MPa (Fig. 19). In the simulated period, steady-state conditions for the pressure field could not be achieved. Productivity Index is an indication of the production potential of a well, and is defined as

$$PI = \frac{Q}{p - p_{wf}} \quad (1)$$

with the flow rate Q , the reservoir pressure p , and flow bottom hole pressure p_{wf} . From the simulation result, PI of the well Gt GrSk 4/05 A2 is calculated as $3.14 \text{ m}^3/(\text{h MPa})$. Injectivity Index follows the same formula but is used for injection wells. From the simulation result, II of the well E GrSk 3/90 is calculated as $1.71 \text{ m}^3/(\text{h MPa})$.

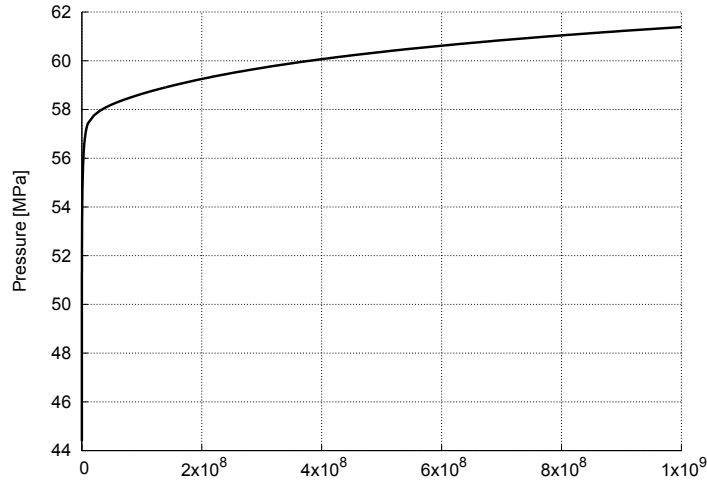


Fig. 18: Pressure profile at the injection point of E GrSk 3/90

For the production temperature, due to the relatively low production and injection rate no significant thermal breakthrough was observed in 30 years (Fig. 20). The temperature rapidly increased to $146.7 \text{ }^\circ\text{C}$ at the beginning and then started decreasing with time. The temperature drop of 1°C was observed after 24 years of the operation, but the temperature does not drop below 140°C at the end of the simulation. As shown in Fig. 21, the injected

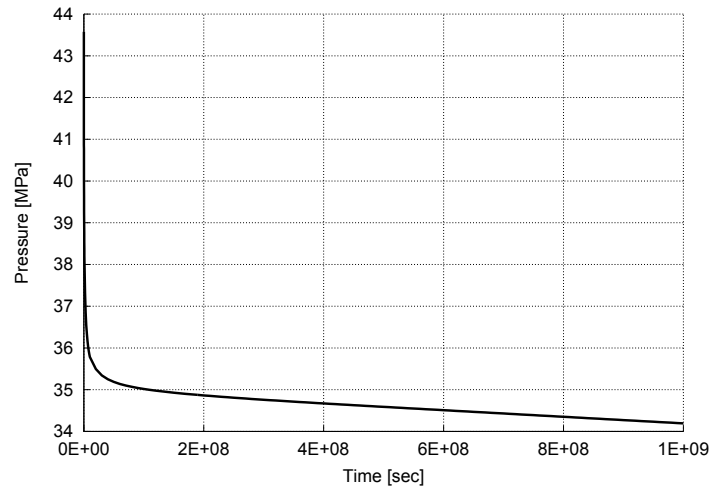


Fig. 19: Pressure profile at the production point of Gt GrSk 4/05

water is heated up along its way from injection to production point. Because the fault zone has high permeability, advective heat transport can be observed along the fault zone.

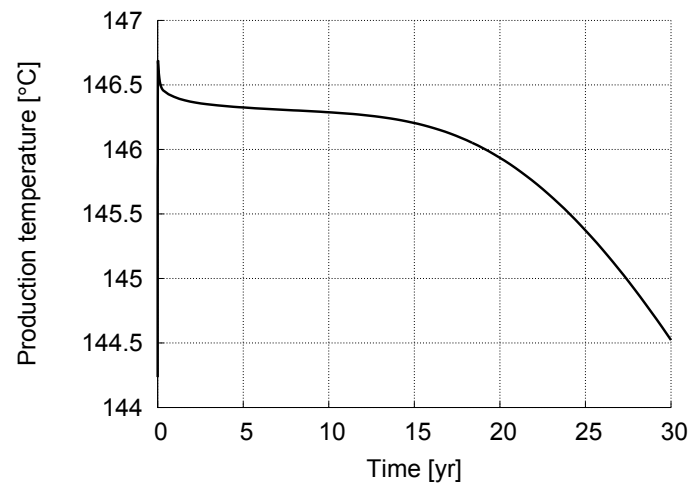


Fig. 20: Temperature profile at the top of the open-hole section of Gt GrSk 4/05

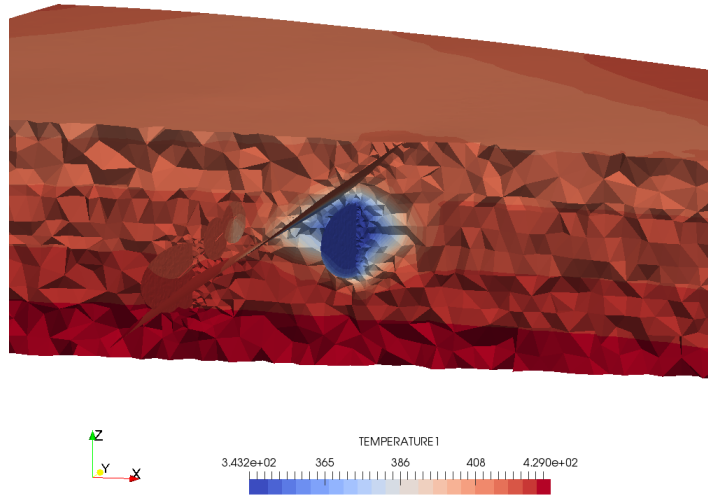


Fig. 21: Simulated temperature distribution after 30 years

Chapter 6

Case Study: Soultz-sous-Forêts

The second case study is given for Soultz-sous-Forêts site in France, which represents an enhanced hydrothermal type of EGS reservoirs. Input files for the simulations are available from <https://docs.opengeosys.org/books/geoenergy-modeling-iii>. Please note that the Soultz data provided can only be used for the scope of this tutorial book and that especially commercial purposes are not allowed.

6.1 Site Description

Geothermal research at Soultz-sous-Forêts site in Alsace, France started in 1986. The site was planned as an Enhanced Geothermal System (EGS) producing energy from a deep-seated heat exchanger allowing the production from initially low permeable basement rocks. More than 20 years of scientific and technical activities in the project provide a large database used in the geothermal community as well as in geoscience in Europe. Since the entering of the industrial consortium GEIE in 2001 economic aspects, besides the scientific research were requested. A pilot power plant, based on the Organic Rankine Cycle (ORC) technology was built in 2008 to start the electricity production (Genter, 2009).

The Soultz site is located next to the western boundary fault of the Upper Rhine Graben (URG), separating graben fillings from basement rocks. The URG is formed in the context of the European Cenozoic rift system in association with the alpine orogenesis (Ziegler, 1994) and is considered as a major mid-european heat anomaly (Baillieux et al, 2013). At the research site, a granitic basement block of N-S orientation is uplifted forming the Soultz horst. The structure is limited to the East and West by Hermerswiller and Kutzenhausen fault zones and covered by only 1400 m of graben sediments of Mesozoic and Cenozoic age. Basements rocks of the horst structure are granitic and can generally be divided in a porphyric monzogranit down to

4800 m separated from a fine grained two-mica granite in greater depth (Hooijkaas et al, 2006) as shown in Fig. 1 (a). The granitic body possess a through intense faulting and fracturing enhanced permeability (Dezayes et al, 2010). Matrix permeability of the fresh granitic body is low, determined in the range of 10^{-16} to 10^{-20} m^2 (Hettkamp et al, 1999; Sardini et al, 1997; Sausse et al, 2006), whereas the secondary permeability is orders of magnitude higher in the range 10^{-15} to 10^{-17} m^2 (Hettkamp et al, 1999) increasing bulk rock permeability.

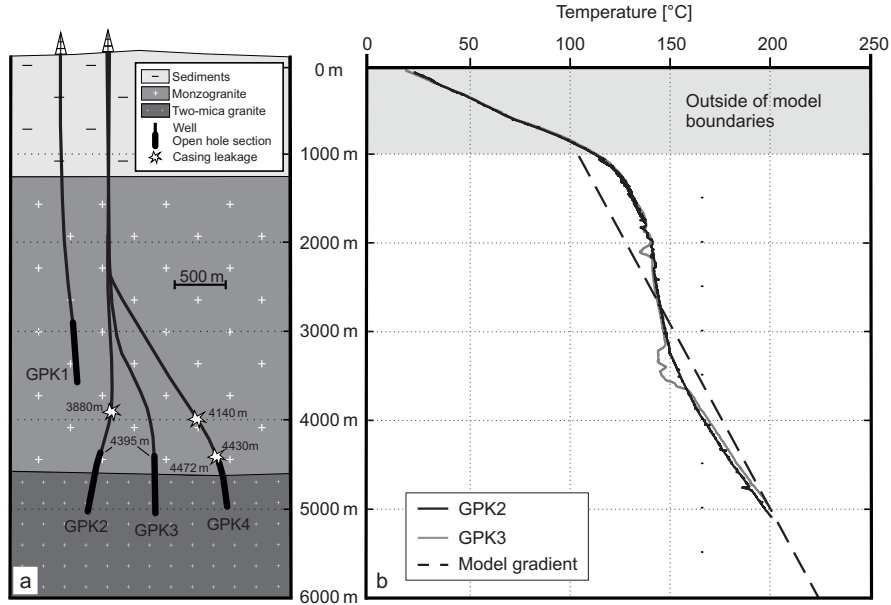


Fig. 1: (a) Simplified deep geology, well trajectories and location of open-hole sections and leakages in the Soultz reservoir, (b) temperature profile in GPK2 and GPK3 and the initial temperature profiles assumed in the numerical model (after Held et al (2014)).⁶

High percentage of fractures following the present-day main horizontal stress of about $170 \pm 14^\circ$ (Cornet et al, 2007). Additional fracture sets, with orientations of $20 \pm 10^\circ$ and $135 \pm 10^\circ$ represent ancient stress direction of Rhenish and Hercynian orogenesis (Dezayes et al, 2010). Fractures are characterized by high inclinations of $> 60^\circ$, dipping mostly to the west. The fault and fracture system, dominating fluid flow, is described in detail by Dezayes et al (2004, 2010). Based on this study a 3-D geological model was created considering also additional geological, petrological and geophysical information (Sausse et al, 2010). This 3-D geological model serves as a basis to construct the here presented numerical model of the Soultz site. As shown

in Fig. 1 (b), the geothermal gradient possess an unusual development with depth. A steep temperature gradient in the sedimentary cap of > 0.1 K/m (Haas and Hoffmann, 1929) is followed by a declined gradient of 0.007 K/m. It is assumed by Le Carlier et al (1994) that the variations in geothermal gradient results from a convection cell between 1000 m and 3500 m depth generating a steep gradient in the graben fillings. Only permeability values as high as $> 10^{-14}$ m² in the fractures in the granitic rock can generate a convection cell as investigated by Bachler et al (2003). Below the base of the convection cell, a typical geothermal gradient of about 0.03 K/m can be observed (Fig. 1 (b)).

The operation of the geothermal reservoir in Soultz is done using four wells drilled in the upper and lower reservoirs in Soultz targeting the wester flank of the Soultz horst without penetrating the horst faults (Soultz, Hermerswiller, Kutzenhausen faults) in the open hole section. (Fig. 1). The western flank of the horst possess an increased electrical conductivity interpreted as a region of intense fracturing and hence increased permeability (Geiermann and Schill, 2010). Three wells (GPK2-4) were drilled into the depth of > 5 km reaching the deep reservoir with temperatures of $> 200^{\circ}\text{C}$. The primary drilled well GPK1 penetrated the lower reservoir at a depth of 3.6 km reaching maximum temperatures of 165°C (Sanjuan et al, 2010). Intensive hydraulic and chemical stimulation in all wells enhanced bulk rock permeability strongly by orders of magnitude (Dorbath et al, 2009; Gérard et al, 1997). The injectivity/productivity of GPK2 was increased by alternating chemical and hydraulic treatment up to twenty-fold (Schindler et al, 2008).

All deep wells are drilled, considering the regional stress pattern, in a direction of $170 \pm 14^{\circ}$, as fractures parallel to that orientation have the potential to remain open and hence increase connectivity between the wells. The three deep wells possess a distance of 650 m in depth, whereas the horizontal distance between GPK1 and GPK2 is 450m. The lowermost 500–700 m of each well are without casing allowing inflow of thermal fluids. Wellbore integrity analysis reveals leakages in GPK2 and GPK4 (Cantini, 2006; Pfender et al, 2006), which are documented in Fig. 1 (a). Mechanisms, causing that damages, are not finally understood, but the coincidences with the location of fracture zones (Dezayes et al, 2004) are remarkable. A combination of post-stimulation shearing and local corrosion could be the origin of decreased wellbore integrity. For the hydraulic flow pattern leakages, especially if created through hydraulically-active fractures, have to be considered. The casing restriction in GPK2 at the depth of 3880 m has to be highlighted as, according to the flow logs, high amounts of fluids entering the well at that depth. The leakage is spatially associated with a large fracture targeting also GPK3 in greater depth (Held et al, 2014). Reservoir flow pattern

⁶ Reprinted from *Geothermics*, Vol. 51, Held S, Genter A, Kohl T, Kolbel T, Sausse J, Schoenball M, Economic evaluation of geothermal reservoir performance through modeling the complexity of the operating EGS in Soultz-sous-Forêts, pp. 270–280, Copyright (2014), with permission from Elsevier.

was investigated after exploration and stimulation of the deeper reservoir using tracer tests (Sanjuan et al, 2006). A fast connection between GPK2 and GPK3 can be demonstrated by fast tracer breakthrough curves. The fast connection could be caused by the fracture zones mentioned above. Low rate of total tracer recovery indicates a mixture of injected with reservoir fluid and lateral fluid movement transporting the injection fluids out of the operated reservoir (Held et al, 2014). Contrary observations were made for the connection between GPK3 and GPK4 where no ideal breakthrough curve is observed and the tracer arrival is delayed and damped (Sanjuan et al, 2006). Fluids, arriving in GPK4, are supposed to originate from a large circulation loop without fast fractures connection between the wells.

6.2 Model Setup

Prior to numerical simulation the existing geological model of Place et al (2011); Sausse et al (2010) has to be simplified and prepared for numerical modeling. Fluid-flow affecting faults and fractures were selected using Flow logs of GPK1-4, partly published by Evans (2005), by identification of the fluid inflow zones. Infiltrating fluids in each well could be easily assigned to a small number of faults. The identification of fractures affecting flow field also considers the orientation of fractures in respect to the regional stress field (Held et al, 2014). Sub-parallel fractures to maximum horizontal stress were preferentially chosen as they are expected to be active for fluid flow (Barton et al, 1995). For the final numerical model, the number of integrated faults and fractures could be minimized to 11, which are presented in Table 2. Those selected structures include the horst faults zones (Kutzenhausen and Hermerwiller) and the dominated Soultz fault zone within the horst structure. The location of complex large-scale faults is taken from Baillieux et al (2013). For simplification, the structure of the faults was reduced to 2-D planar surfaces. Inside the reservoir, the 7 selected fractures, important for fluid flow, were all cutoff by the dominate fracture GPK-FZ4770* connecting GPK2 and GPK3 or by fault zones. To consider hydraulic and chemical stimulation GPK-FZ4770* was subdivided next to the intersection with GPK2 and GPK3 allowing the assignment of higher permeabilities for the stimulated areas. The fault and fractures were extended to model boundaries or until they are cutoff by a more dominate structure, in order to create a connected fracture network. A connection of open hole sections to the fracture and fault network is ensured by two fractures per well except for GPK1, where the 3-D geological model present only one hydraulical active fracture cutting the open hole section.

In the numerical model, we consider a domain with extensions of 13 km (E-W), 11 km (N-S) and 5 km (vertical) (Fig. 2). Thus a lateral distance of at least 4 km from each open hole section to the model boundaries is en-

sured hindering a direct impact of the imposed boundary conditions. Vertical extension is from 1 km reaching 6 km depth. The minimum vertical distance between wells and boundaries is 1 km. The sedimentary graben fillings, reaching a depth of 1.4 km at the Soultz horst, are not considered in the model as the granitic rock matrix is assumed up to the top. No major interactions between the wells and the sediments above the reservoir are observed from numerical modeling, also in depth shallower as 1 km.

A finite element mesh for the defined domain (Fig. 2) was generated using the software Hypermesh (Altair Engineering, Inc.), and is available from the tutorial website. The 3-D mesh consists of tetrahedrons representing the rock matrix. Fault and fractures are implemented by triangular elements arranged on 2-D surfaces. Open hole parts of the wells are represented by 1-D line elements. Casing leakages, occurring above the open hole sections, are connected to the open-hole sections by extended line elements crosscutting rock matrix without interaction. Meshing was performed adapted to the complexity of geometry and expected gradient. Elements on the fracture surfaces at the connection to the wells have sizes of less than 3 m, whereas the far field tetrahedrons possess the maximum length of 500 m.

Simulation of in-situ pressure distribution was imposed by Dirichlet boundary conditions at lateral model boundaries (Fig. 3) representing hydrostatic conditions. Fluid density was set to 1065 kg/m^3 (Sanjuan et al, 2010). Convection cell affected geothermal gradient was reproduced by an artificial linear temperature gradient of 0.024 K/m by setting Dirichlet temperature boundary conditions on top and bottom model surfaces (Fig. 3). Artificial temperature gradient was set to minimize temperature difference between model and in-situ measurements especially in the open-hole and central part of the reservoir area. Unperturbed initial pressure and temperature conditions are obtained by steady state simulation using the above described boundary conditions. Therefore hydraulic and thermal initial conditions are determined separately assuming homogeneous hydraulic parameters to calculate hydraulic initial conditions.

The operation is simulated by extraction of reservoir fluid from GPK2 assuming a production rate of 26 l/s (Held et al, 2014). The cooled fluid is re-injected into the reservoir via GPK1 and GPK3 with injection rates of 13 l/s and 10 l/s respectively. The misfit between produced and injected volumes is provoked by the density contrast generated mainly by heat extraction within the power plant process. The fluid after withdrawal of heat inside the power plant has a temperature of 70°C used as injection temperature in GPK1 and GPK3. Production and injection rates are implemented using Neumann type boundary condition. In the numerical simulations, we compute a stationary pressure field only once to save computation time as production and injection rates are not transient. Temperature field is solved as a transient process. Fluid density contrasts and turbulent flow are not considered in this simulations. Fluid viscosity is temperature-dependent (Ramey et al, 1974) as

$$\mu = 2.394 \cdot 10^{\left[\frac{248.37}{T + 133.15} \right]} \cdot 10^{-5}$$

where temperature T here is in Celsius. All the parameters used in the simulations are listed in Table 1, Table 2, and Table 3.

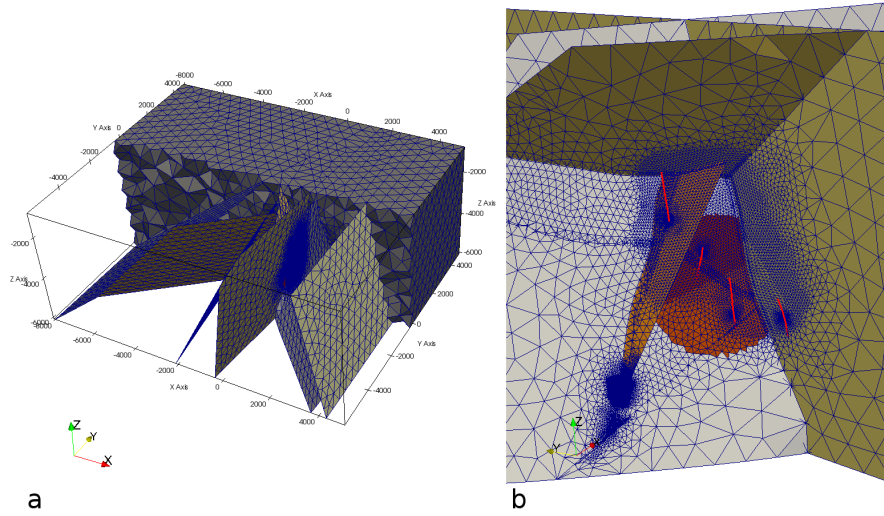


Fig. 2: a) Semi-uncovered finite element mesh with 100,260 nodes and 628,052 elements (704 lines, 44,249 triangles, 583,099 tetrahedron). Matrix, consisting of 3-D tetrahedrons, contains 2-D surfaces, generated by 2-D triangular elements, representing fractures. b) Detailed view of reservoir including open hole sections of the four wells (red line elements) and major fractures.

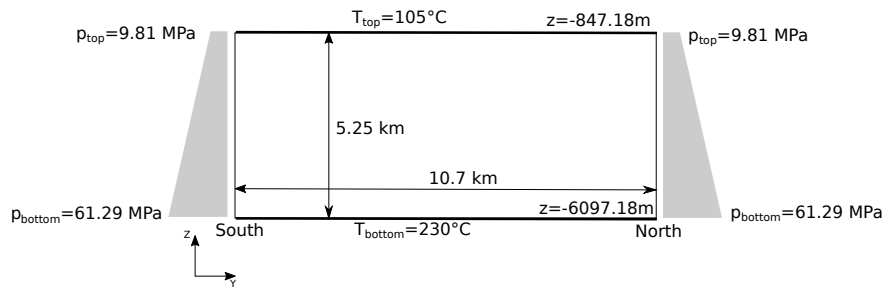


Fig. 3: In-situ boundary conditions

Property	Value
Production rate at GPK2	26 L/s
Injection rate at GPK3	10 L/s
Injection rate at GPK1	13 L/s
Injection temperature	70 °C
Rock permeability	10^{-15} m ²
Rock porosity	1 %
Rock density	2600 kg/m ³
Rock specific heat capacity	850 J/kg/K
Rock thermal conductivity	3.0 W/m/K
Rock storage	0 Pa ⁻¹
Fluid density	1065 kg/m ³
Fluid viscosity	Ramey et al (1974)
Fluid specific heat capacity	4200 J/kg/K
Fluid thermal conductivity	0.6 W/m/K
Temperature at the top	105 °C
Temperature at the bottom	230 °C
Pore pressure at the top	9.81 MPa
Pore pressure at the bottom	61.29 MPa

Table 1: Model parameters

Mat. ID	Fault/Fracture	Aperture [m]	Porosity [-]	Storage [Pa ⁻¹]	Permeability [m ²]
0	GPK3-FZ4770*	0.01	1.0	0.0	10^{-11}
1	Kutzenhausen	0.01	1.0	0.0	$5 \cdot 10^{-10}$
2	Soultz	0.01	1.0	0.0	$5 \cdot 10^{-10}$
3	Hermerswiller	0.01	1.0	0.0	$5 \cdot 10^{-10}$
4	MS-GPK4-20045b	0.01	1.0	0.0	10^{-12}
5	GPK2-FZ2120	0.01	1.0	0.0	10^{-12}
6	PS3-int (VSP)	0.01	1.0	0.0	10^{-12}
7	GPK4-FZ4710	0.01	1.0	0.0	10^{-12}
8	MS-GPK3-2003a	0.01	1.0	0.0	10^{-12}
9	GPK3-FZ5020	0.01	1.0	0.0	10^{-12}
10	MS-GPK2-2000a	0.01	1.0	0.0	10^{-12}
11	GPK3-FZ4770* near GPK2	0.01	1.0	0.0	10^{-11}
12	GPK3-FZ4770* near GPK3	0.01	1.0	0.0	10^{-11}

Table 2: Fault parameters.

Mat. ID	Wellbore	Cross sectional area [m]	Porosity [-]	Storage [Pa ⁻¹]	Permeability [m ²]
13	GPK1	3.66E-2	1.0	0.0	1E-6
14	GPK2	3.66E-2	1.0	0.0	1E-6
15	GPK3	1.98E-2	1.0	0.0	1E-6
16	GPK4	3.66E-2	1.0	0.0	1E-16

Table 3: Wellbore parameters. Permeability of GPK4 is set to 10^{-16} , as the well is not considered in the selected operation scenario.

6.3 Simulation of Initial Reservoir Conditions

Numerical modeling, after implementing the given mesh file, starts by computing initial conditions, i.e. undisturbed state, of the reservoir. We simulate steady-state pressure and temperature distributions without considering fluid circulation and use its results as initial conditions for the heat extraction simulations. The following subsections explain OGS input files for the steady state simulation.

6.3.1 Input Files

GLI - geometry

The GLI file defines points, polylines, and outer domain surfaces which are used for boundary conditions and result outputs.

Listing 6.1: A part of the GLI input file

```
#POINTS
0 5017 4806 -847.18 $NAME NOo
1 5017 4806 -6097.18 $NAME NOu
2 5017 -5894 -6097.18 $NAME SOu
3 5017 -5894 -847.18 $NAME SOo
4 -8083 -5894 -847.18 $NAME SWo
5 -8083 -5894 -6097.18 $NAME SWu
6 -8083 4806 -847.18 $NAME NWo
7 -8083 4806 -6097.18 $NAME NWu
8 51.260000000009 -108.31 -2542.89458 $NAME GPK1
9 193.66125 -532.75 -3552.103072266 $NAME GPK2
10 153.92199218995 -932.1660156199 -3899.329390625 $NAME GPK3
11 297.359999999999 -1528.165 -4129.41093 $NAME GPK4
#POLYLINE
$NAME
Sued
$POINTS
2
3
4
5
2
#POLYLINE
```

PCS - process definition

A steady-state simulation can be specified in `$TIM_TYPE` with `STEADY` keyword. The well elements (Material IDs 13–16) has to be excluded from the simulation by setting `$DEACTIVATED_SUBDOMAIN`. To let OGS generate restart files, `$RELOAD` keyword has to be provided with a mode 1.

Listing 6.2: PCS input file

```

#PROCESS
$PCS_TYPE
LIQUID_FLOW
$TIM_TYPE
STEADY
$DEACTIVATED_SUBDOMAIN
4
13 14 15 16
$RELOAD
1 1
#PROCESS
$PCS_TYPE
HEAT_TRANSPORT
$TIM_TYPE
STEADY
$DEACTIVATED_SUBDOMAIN
4
13 14 15 16
$RELOAD
1 1
#STOP

```

NUM - numerical properties

The NUM file should be configured as shown in Listing 6.3.

Listing 6.3: NUM input file

```

$OVERALL_COUPLING
;min_iter -- max_iter
1 25
#NUMERICS
$PCS_TYPE
LIQUID_FLOW
$LINEAR_SOLVER
; method error_tolerance max_iterations theta precondition storage
9 6 1.e-012 3000 1.0 9 4
$NON_LINEAR_ITERATIONS
;type -- error_method -- max_iterations -- relaxation -- tolerance(s)
PICARD LMAX 1 1 10
$COUPLING_CONTROL
;error method -- tolerances
LMAX 10
#NUMERICS
$PCS_TYPE
HEAT_TRANSPORT
$LINEAR_SOLVER
; method error_tolerance max_iterations theta precondition storage
9 6 1.e-012 3000 1.0 9 4
$NON_LINEAR_ITERATIONS
;type -- error_method -- max_iterations -- relaxation -- tolerance(s)
PICARD LMAX 1 1 1e-3
$COUPLING_CONTROL
;error method -- tolerances
LMAX 1.e-3
$ELE_MASS_LUMPING
1
$ELE_SUPG
1 0 0

```

```
#STOP
```

TIM - time discretization

For steady state, only one time step is required.

Listing 6.4: TIM input file

```
#TIME_STEPPING
$PCS_TYPE
  LIQUID_FLOW
$TIME_START
  0
$TIME_END
  1
$TIME_STEPS
  1 1
#TIME_STEPPING
$PCS_TYPE
  HEAT_TRANSPORT
$TIME_START
  0
$TIME_END
  1
$TIME_STEPS
  1 1
#STOP
```

IC - initial conditions

We need to provide initial conditions, because some of the deactivated well-bore element nodes are not shared by matrix elements and their values will not be computed in the simulation. Reasonable initial values are still required for those nodes because they are included in restart files for the transient simulation. Here we set depth-dependent linear distributions of both pressure and temperature assuming a fluid density of 1065 kg/m^3 and a geothermal gradient of 0.0238 K/m . These are consistent with the boundary conditions. Distribution type `$GRADIENT` can be used for this purpose.

Listing 6.5: IC input file

```
#INITIAL_CONDITION
$PCS_TYPE
  LIQUID_FLOW
$PRIMARY_VARIABLE
  PRESSURE1
$GEO_TYPE
  DOMAIN
$DIS_TYPE
  GRADIENT -847.18 9810000 10447.65 ; rho_f = 1065
#INITIAL_CONDITION
$PCS_TYPE
```

```

HEAT_TRANSPORT
$PRIMARY_VARIABLE
TEMPERATURE1
$GEO_TYPE
DOMAIN
$DIS_TYPE
GRADIENT -847.18 378.15 0.0238
#STOP

```

BC - boundary conditions

In the BC input file, prescribed values have to be provided. In this example, we set hydrostatic pressure at the lateral boundaries and prescribed temperature at the top and bottom surfaces. The hydrostatic pressure distribution is linearly depth-dependent and therefore is given by using `$GRADIENT` keyword.

Listing 6.6: BC input file

```

#BOUNDARY_CONDITION
$PCS_TYPE
LIQUID_FLOW
$PRIMARY_VARIABLE
PRESSURE1
$GEO_TYPE
SURFACE Sued1
$DIS_TYPE
GRADIENT -847.18 9810000 10447.65 ; rho_f = 1065
#BOUNDARY_CONDITION
$PCS_TYPE
LIQUID_FLOW
$PRIMARY_VARIABLE
PRESSURE1
$GEO_TYPE
SURFACE Nord1
$DIS_TYPE
GRADIENT -847.18 9810000 10447.65 ; rho_f = 1065
#BOUNDARY_CONDITION
$PCS_TYPE
HEAT_TRANSPORT
$PRIMARY_VARIABLE
TEMPERATURE1
$GEO_TYPE
SURFACE Unten
$DIS_TYPE
CONSTANT 503.15
#BOUNDARY_CONDITION
$PCS_TYPE
HEAT_TRANSPORT
$PRIMARY_VARIABLE
TEMPERATURE1
$GEO_TYPE
SURFACE Oben
$DIS_TYPE
CONSTANT 378.15
#STOP

```

MFP - fluid properties

In the MFP input file, we specify the Ramey et al (1974) model to fluid viscosity and set constant values to fluid density, specific heat, and thermal conductivity.

Listing 6.7: MFP input file

```
#FLUID_PROPERTIES
$DENSITY
1 1065
$VISCOSITY
22 ; Ramey (1974)
$SPECIFIC_HEAT_CAPACITY
1 4200
$HEAT_CONDUCTIVITY
1 0.6
#STOP
```

MSP - solid properties

The MSP input file contain solid phase parameters for the rock matrix, the faults, the fractures, and the wells. For all the faults, fractures, and wells, we set some dummy values as below, because their porosity is assumed to be one.

Listing 6.8: Matrix definition example in MSP input file

```
; Matrix
#SOLID_PROPERTIES
$DENSITY
1 2600
$THERMAL
EXPANSION
6.0e-6
CAPACITY
1 850
CONDUCTIVITY
1 3.0
```

For the rock matrix, the definition should be given as specified in Table 1.

Listing 6.9: Fracture definition example in MSP input file

```
; fracture GPK3-FZ4770
#SOLID_PROPERTIES
$DENSITY
1 1000
$THERMAL
EXPANSION
6.0e-6
CAPACITY
1 4200
CONDUCTIVITY
1 0.6
```

MMP - porous medium properties

In the MMP input file, medium properties have to be provided according to Table 1, Table 2, and Table 3. Examples are shown below. For simplification, fault and fracture permeabilities are set to default values. Effects of permeability changes can be investigated during the exercises.

Listing 6.10: Fracture definition example in MMP input file

```

; fracture GPK3-FZ4770
#MEDIUM_PROPERTIES
$GEOMETRY_DIMENSION
2
$GEOMETRY_AREA
1e-2
$POROSITY
1 1.0
$STORAGE
1 0
$PERMEABILITY_TENSOR
ISOTROPIC 1.00e-11

```

Listing 6.11: Wellbore definition example in MMP input file

```

#MEDIUM_PROPERTIES
$GEOMETRY_DIMENSION
1
$GEOMETRY_AREA
3.66e-2
$POROSITY
1 1.0
$STORAGE
1 0
$PERMEABILITY_TENSOR
ISOTROPIC 1.00e-6

```

Listing 6.12: Matrix definition example in MMP input file

```

#MEDIUM_PROPERTIES
$GEOMETRY_DIMENSION
3
$GEOMETRY_AREA
1.0
$POROSITY
1 0.01
$STORAGE
1 0
$PERMEABILITY_TENSOR
ORTHOTROPIC 1.00e-15 1.00e-15 1.00e-15

```

OUT - output parameters

In the OUT input file, we define output of results for the entire domain in PVD and VTU files, and outputs of time-series values at the top of the wellbores in CSV files.

Listing 6.13: OUT input file

```
#OUTPUT
$NOD_VALUES
  PRESSURE1
  TEMPERATURE1
$ELE_VALUES
  VELOCITY1_X
$MFP_VALUES
  DENSITY
  VISCOSITY
$GEO_TYPE
  DOMAIN
$DAT_TYPE
  PVD
$TIM_TYPE
  STEPS 1
#OUTPUT
$NOD_VALUES
  PRESSURE1
  TEMPERATURE1
$GEO_TYPE
  POINT GPK2
$DAT_TYPE
  CSV
$TIM_TYPE
  STEPS 1
#OUTPUT
$NOD_VALUES
  PRESSURE1
  TEMPERATURE1
$GEO_TYPE
  POINT GPK3
$DAT_TYPE
  CSV
$TIM_TYPE
  STEPS 1
#OUTPUT
$NOD_VALUES
  PRESSURE1
  TEMPERATURE1
$GEO_TYPE
  POINT GPK1
$DAT_TYPE
  CSV
$TIM_TYPE
  STEPS 1
#STOP
```

6.3.2 Results

After executing OGS with the above input files, one should obtain PVD/VTU files and the following restart files which are used in the next transient simulation.

- Sultz_LIQUID_FLOW_PRESSURE1_primary_value_1.asc.
- Sultz_HEAT_TRANSPORT_TEMPERATURE1_primary_value_1.asc.

Simulated steady-state pressure and temperature fields can be visualized with ParaView as shown in Fig. 4. Using *PlotOverLine* filter, one can plot vertical profiles of the values (see Fig. 5).

As shown in the figure, simulated temperature is closely matching the measured profile in GPK2 although it linearly distributes with the depth. The linear gradient was artificially imposed by the Dirichlet boundary conditions at the top and bottom surfaces. The misfit between unperturbed reservoir temperature and model temperature is 18 K near the upper part of the model, where the natural temperature gradient is high. The temperature in the sedimentary cover is slightly underestimated, whereas an overestimation for the temperature in deeper parts is evident. However, as the artificial gradient was designed to minimize misfit between in-situ and model data, the heat distribution in the central part of the reservoir match the natural conditions best possible.

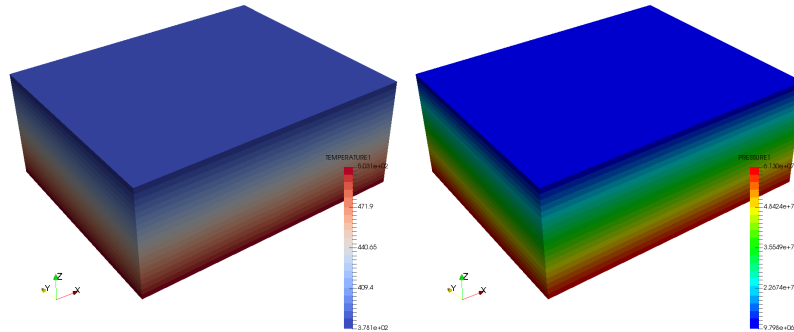


Fig. 4: Simulated initial temperature and pressure distributions

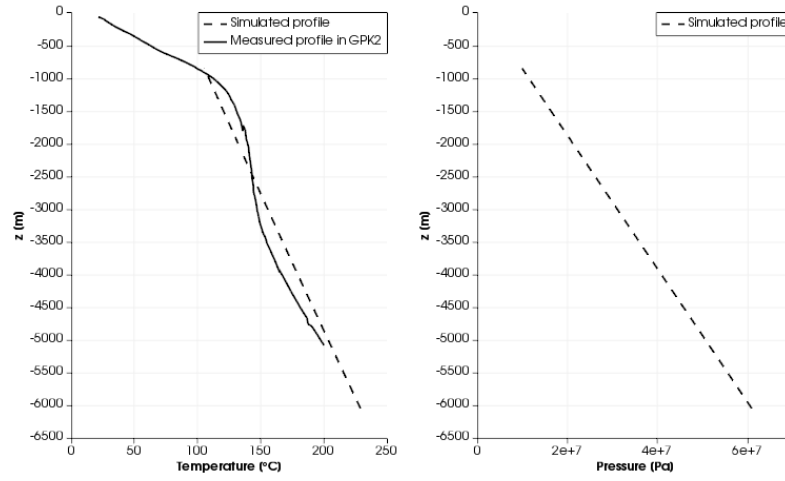


Fig. 5: Vertical profiles of initial temperature and pressure

6.4 Simulation of Heat Extraction Process

Prior to transient simulation, we have to copy the restart files generated during steady-state simulation to the working directory for the transient simulation. To help OGS detect the restart files, we have to remove ”_1” from the restart file names. Having the renamed restart files, we are ready to simulate transient reservoir operation. An implementation of transient hydraulic simulation was renounced to reduce calculation time but could be easily integrated to simulate time-dependent operation. The following sections explain only the input files which are different from the steady-state simulation.

6.4.1 Input Files

PCS - process definition

To use the restart files as initial conditions, \$RELOAD has to be changed to mode 2.

Listing 6.14: PCS input file

```
#PROCESS
  $PCS_TYPE
    LIQUID_FLOW
  $RELOAD
    2
#PROCESS
  $PCS_TYPE
    HEAT_TRANSPORT
  $RELOAD
    2
#STOP
```

TIM - time discretization

Simulation time is set to 30 years as, for economic considerations, lifetime of investments is assumed to 30 years (Held et al, 2014). As the system behavior is highly dynamic at the beginning of the simulation, time stepping is started with a very small length and is gradually increased.

Listing 6.15: A part of the TIM input file

```
#TIME_STEPPING
  $PCS_TYPE
    LIQUID_FLOW
  $TIME_START
    0
  $TIME_END
```

```

1000000000
$TIME_STEPS
10 0.001
 9 0.01
 9 0.1
 9 1
 9 10
 9 100
 9 1000
 9 10000
 9 100000
 9 1000000
99 10000000

```

BC - boundary conditions

For the transient simulation, re-injection temperature of 70°C is set at the injection well points in GPK1 and GPK3, complementing thermal boundary conditions.

Listing 6.16: New additions in the BC input file

```

$PCS_TYPE
HEAT_TRANSPORT
$PRIMARY_VARIABLE
TEMPERATURE1
$GEO_TYPE
POINT GPK1
$DIS_TYPE
CONSTANT 343.15
#BOUNDARY_CONDITION
$PCS_TYPE
HEAT_TRANSPORT
$PRIMARY_VARIABLE
TEMPERATURE1
$GEO_TYPE
POINT GPK3
$DIS_TYPE
CONSTANT 343.15

```

ST - source/sink terms

Production and injection rates are implemented with Neumann-type boundary conditions at the uppermost node of each well.

Listing 6.17: ST input file

```

#SOURCE_TERM
$PCS_TYPE
LIQUID_FLOW
$PRIMARY_VARIABLE
PRESSURE1
$GEO_TYPE
POINT GPK2

```

```

$DIS_TYPE
  CONSTANT -0.026
#SOURCE_TERM
$PCS_TYPE
  LIQUID_FLOW
$PRIMARY_VARIABLE
  PRESSURE1
$GEO_TYPE
  POINT GPK3
$DIS_TYPE
  CONSTANT 0.01
#SOURCE_TERM
$PCS_TYPE
  LIQUID_FLOW
$PRIMARY_VARIABLE
  PRESSURE1
$GEO_TYPE
  POINT GPK1
$DIS_TYPE
  CONSTANT 0.013
#STOP

```

6.4.2 Results

After executing OGS with the above shown input files, one should obtain PVD/VTU files for distributed values for every 5th time step and CSV files for time profiles at the injection and production points.

The temperature development of the produced fluid in GPK2 (Fig. 6) shows an initial temperature increase to 175°C. This increase can be explained by fluid inflow from deeper sections of the reservoir and was confirmed by observations at the Soultz site. Furthermore, no temperature drawdown is apparent within the simulated period of 30 years (Fig. 6).

Fig. 7 shows spatial temperature distribution along the fractures in the reservoir. The impact of cooling due to re-injection of fluids is clearly visible. The cooling occurs mostly on fracture zones and do not effect, even after 30 years of operation, the production in GPK2.

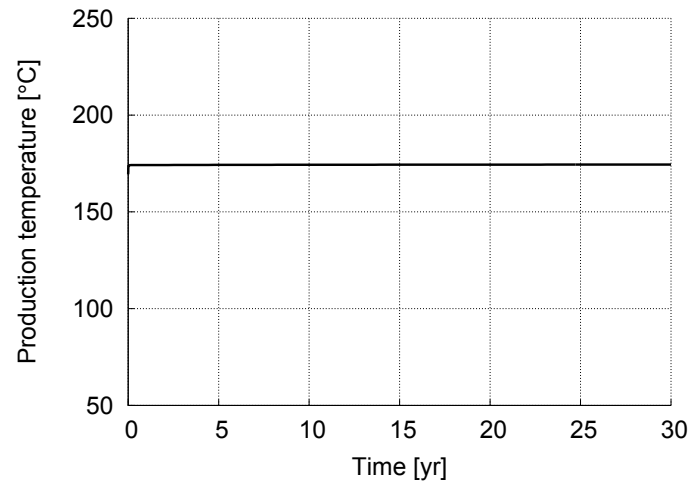


Fig. 6: Temporal profile of production temperature at GPK2

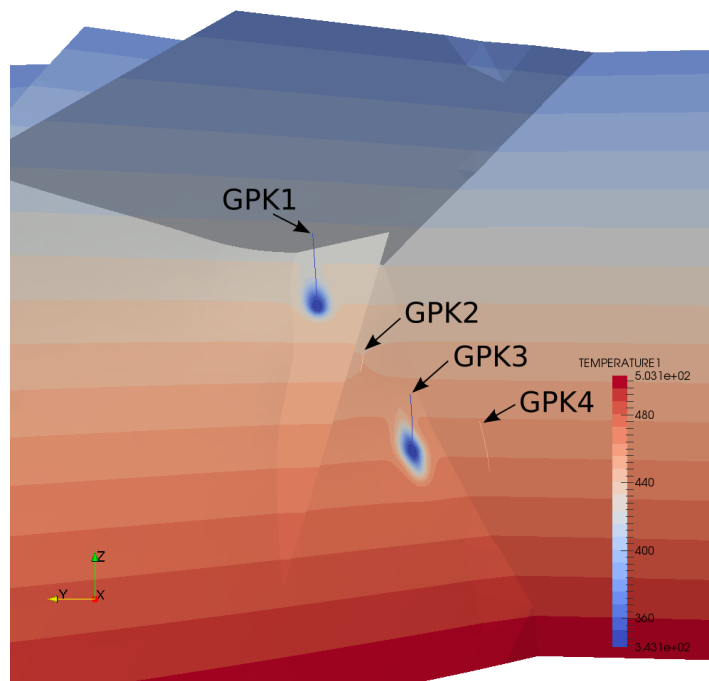


Fig. 7: Simulated temperature distribution after 31.7 years.

Appendix A

Keywords

This section provides a wrap-up compendium of the OGS keywords used in this tutorial. A more comprehensive compilation of OGS keywords you can find at <https://svn.ufz.de/ogs/wiki/public/doc-auto>.

GLI - geometry

Listing A.1: GLI keyword

```
#POINTS          // points keyword
0 0 0 0 $NAME POINT0 // point number | x | y | z | point name
1 1 0 0 $NAME POINT1 // point number | x | y | z | point name
#POLYLINE        // polyline keyword
$NAME            // polyline name subkeyword
LINE            // polyline name
$POINTS          // polyline points subkeyword
0               // point of polyline
1               // dito
#STOP           // end of input data
```

MSH - finite element mesh

Listing A.2: MSH keyword

```
#FEM_MSH        // file/object keyword
$NODES          // node subkeyword
61              // number of grid nodes
0 0 0 0         // node number x y z
1 0 0 1         // dito
...
59             0           0           59
60             0           0           60
```

```

$ELEMENTS      // element subkeyword
60             // number of elements
0              line 0 1 // element number | material group
              number | element type | element node numbers
1              line 1 2 // dito
...
58             line 58 59 // dito
59             line 59 60 // dito
#STOP          // end of input data

```

PCS - process definition

Listing A.3: PCS keyword

```

#PROCESS       // process keyword
$PCS_TYPE     // process type subkeyword
HEAT_TRANSPORT // specified process(es)
LIQUID_FLOW   // dito
...
#STOP         // end of input data

```

NUM - numerical properties

Listing A.4: NUM keyword

```

#NUMERICS     // process keyword
$PCS_TYPE     // process type subkeyword, see PCS above
$LINEAR_SOLVER // linear solver type subkeyword, see table below
Parameters    // 7 parameters, see table below
#STOP         // end of input data

```

TIM - time discretization

Listing A.5: TIM keyword

```

#TIME_STEPPING // timt stepping keyword
$PCS_TYPE     // process subkeyword
HEAT_TRANSPORT // specified process
$TIME_STEPS   // time steps subkeyword
1000 390625e+0 // number of times steps | times step length
$TIME_END     // end time subkeyword
1E99         // end time value
$TIME_START   // starting time subkeyword

```

```

0.0          // starting time value
$TIME_UNIT  // specified time unit
  DAY       // SECOND, DAY, YEAR
#STOP      // end of input data

```

IC - initial conditions

Listing A.6: IC keyword

```

#INITIAL_CONDITION // initial conditions keyword
$PCS_TYPE          // process subkeyword
  HEAT_TRANSPORT  // specified process
$PRIMARY_VARIABLE // primary variable subkeyword
  TEMPERATURE1   // specified primary variable
$GEO_TYPE          // geometry subkeyword
  DOMAIN         // specified geometry: entire domain (all nodes)
$DIS_TYPE          // distribution subkeyword
  CONSTANT 0     // specified distribution: constant value 0 at DOMAIN
                  geometry
#STOP             // end of input data

```

BC - boundary conditions

Listing A.7: BC keyword

```

#BOUNDARY_CONDITION // boundary condition keyword
$PCS_TYPE           // process type subkeyword
  HEAT_TRANSPORT   // specified process
$PRIMARY_VARIABLE   // primary variable subkeyword
  TEMPERATURE1     // specified primary variable
$GEO_TYPE           // geometry type subkeyword
  POINT POINTO     // specified geometry type | geometry name
$DIS_TYPE           // boundary condition type subkeyword
  CONSTANT 1       // boundary condition type | value
#STOP              // end of input data

```

ST - source/sink terms

Listing A.8: ST keyword

```

#SOURCE_TERM      // source term keyword
$PCS_TYPE         // process type subkeyword
  LIQUID_FLOW     // specified process

```

```

$PRIMARY_VARIABLE // primary variable subkeyword
PRESSURE1 // specified primary variable
$GEO_TYPE // geometry type subkeyword
POINT POINTO // specified geometry type | geometry name
$DIS_TYPE // boundary condition type subkeyword
CONSTANT_NEUMANN 1E-6 // source term type | value
#STOP // end of input data

```

MFP - fluid Properties

Listing A.9: MFP keyword

```

#FLUID_PROPERTIES // fluid properties keyword
$DENSITY // fluid density subkeyword
4 1000 0 -0.2 // type (4: temperature dependent) | 2 values
$VISCOSITY // fluid viscosity subkeyword
1 0.001 // type (1: constant value) | value
$SPECIFIC_HEAT_CAPACITY // specific heat capacity subkeyword
1 4200.0 // type (1: constant value) | value
$HEAT_CONDUCTIVITY // thermal heat conductivity subkeyword
1 0.65 // type (1: constant value) | value
#STOP // end of input data

```

MSP - solid properties

Listing A.10: MSP keyword

```

#SOLID_PROPERTIES // solid properties keyword
$DENSITY // solid density subkeyword
1 2500 // type (1: constant value) | value
$THERMAL // thermal properties subkeyword
EXPANSION: // thermal expansion
1.0e-5 // values
CAPACITY: // heat capacity
1 1000 // type (1: constant value) | value
CONDUCTIVITY: // thermal conductivity
1 3.2 // type (1: constant value) | value
#STOP // end of input data

```

MMP - porous medium properties

Listing A.11: MMP keyword

```

#MEDIUM_PROPERTIES // solid properties keyword
$GEOMETRY_DIMENSION // dimension subkeyword
1 // 1: one-dimensional problem
$GEOMETRY_AREA // geometry area subkeyword
1.0 // value in square meter if 1D
$POROSITY // porosity subkeyword
1 0.10 // type (1: constant value) | value
$STORAGE // storativity subkeyword
1 0.0 // type (1: constant value) | value
$TORTUOSITY // tortuosity subkeyword
1 1.000000e+000 // type (1: constant value) | value
$PERMEABILITY_TENSOR // permeability subkeyword
ISOTROPIC 1.0e-15 // tensor type (ISOTROPIC) | value(s)
$HEAT_DISPERSION // porosity subkeyword
1 0.0e+00 0.0e+00 // type (1: constant values) | longitudinal |
transverse // thermal dispersion length
#STOP // end of input data

```

OUT - output parameters

Listing A.12: OUT keyword

```

#OUTPUT // output keyword
$PCS_TYPE // process subkeyword
HEAT_TRANSPORT // specified process
$NOD_VALUES // nodal values subkeyword
TEMPERATURE1 // specified nodal values
$GEO_TYPE // geometry type subkeyword
POLYLINE ROCK // geometry type and name
$TIM_TYPE // output times subkeyword
STEPS 1 // output methods and parameter
#STOP // end of input data

```


References

- Bachler D, Kohl T, Rybach L (2003) Impact of graben-parallel faults on hydrothermal convection - Rhine Graben case study. *Physics and Chemistry of the Earth* 28(9-11):431–441
- Baillieux P, Schill E, Edel JB, Mauri G (2013) Localization of temperature anomalies in the Upper Rhine Graben: insights from geophysics and neotectonic activity. *International Geology Review* 55(14):1744–1762
- Barenblatt G, Zheltov I, Kochina I (1960) Basic concepts in the theory of seepage of homogeneous liquids in fissured rocks (strata). *Journal of Applied Mathematics and Mechanics* 24:1286–1303
- Barton CA, Zoback MD, Moos D (1995) Fluid-flow along potentially active faults in crystalline rock. *Geology* 23(8):683–686
- Blöcher G, Cacace M, Reinsch T, Watanabe N (2015) Evaluation of three exploitation concepts for a deep geothermal system in the North German Basin. *Computers & Geosciences* 82:120–129
- Blöcher MG, Zimmermann G, Moeck I, Brandt W, Hassanzadegan A, Magri F (2010) 3D numerical modeling of hydrothermal processes during the lifetime of a deep geothermal reservoir. *Geofluids* 10(3):406–421
- Böttcher N, Watanabe N, Görke U, Kolditz O (2016) *Geoenergy Modeling I - Geothermal Processes in Fractured Porous Media*. Springer
- Cacace M, Blöcher G (2015) MeshIt-a software for three dimensional volumetric meshing of complex faulted reservoirs. *Environmental Earth Sciences* 74(6):5191–5209
- Cantini S (2006) GEIE Well GPK-4 Flow Log - Leak Detection, Technical Report Schlumberger for GEIE EMC. Tech. rep.
- Cornet FH, Berard T, Bourouis S (2007) How close to failure is a granite rock mass at a 5 km depth? *International Journal of Rock Mechanics and Mining Sciences* 44(1):47–66
- Dezayes C, Genter A, Gentier S (2004) Fracture network of the EGS geothermal reservoir at Soultz-sous-Forêts (Rhine Graben, France). In: *Geothermal Resources Council*, 213–218. Palm Springs, CA, USA.

- Dezayes C, Genter A, Valley B (2010) Structure of the low permeable naturally fractured geothermal reservoir at Soultz. *Comptes Rendus Geoscience* 342(7-8):517–530
- Dickson MH, Fanelli M (2004) What is geothermal energy? Tech. rep., Istituto di Geoscienze e Georisorse, Pisa, Italy
- Diersch HJ (2002) FEFLOW Finite Element Subsurface Flow and Transport Simulation System – User’s Manual/Reference Manual/White Papers (2002), Release 5.0. Tech. rep., WASY Ltd, Berlin.
- DiPippo R (2012) *Geothermal Power Plants*, 3rd Edition. Elsevier
- Dorbath L, Cuenot N, Genter A, Frogneux M (2009) Seismic response of the fractured and faulted granite of Soultz-sous-Forêts (France) to 5 km deep massive water injections. *Geophysical Journal International* 177(2):653–675
- Evans KF (2005) Permeability creation and damage due to massive fluid injections into granite at 3.5 km at Soultz: 2. Critical stress and fracture strength. *Journal of Geophysical Research: Solid Earth* 110(B4), b04204
- Franco A, Vaccaro M (2014) Numerical simulation of geothermal reservoirs for the sustainable design of energy plants: A review. *Renewable and Sustainable Energy Reviews* 30:987–1002
- Frick S, Regenspurg S, Kranz S, Milsch H, Saadat A, Francke H, Brandt W, Huenges E (2011) Geochemical and process engineering challenges for geothermal power generation. *Chemie Ingenieur Technik* 83(12):2093–2104
- Geiermann J, Schill E (2010) 2-D Magnetotellurics at the geothermal site at Soultz-sous-Forêts: Resistivity distribution to about 3000 m depth. *Comptes Rendus Geoscience* 342(7-8):587–599
- Genter A (2009) EGS PILOT PLANT Publishable Final Activity Report. Tech. rep.
- Genter A, Cuenot N, Goerke X, Melchert B, Sanjuan B, Scheiber J (2012) Status of the Soultz geothermal project during exploitation between 2010 and 2012. In: 37th Workshop on Geothermal Reservoir Engineering. Stanford University, CA, USA.
- Geuzaine C, Remacle JF (2009) Gmsh: A 3-D finite element mesh generator with built-in pre- and post-processing facilities. *International Journal for Numerical Methods in Engineering* 79(11):1309–1331
- Guvanasen V, Chan T (2000) A three-dimensional numerical model for thermohydromechanical deformation with hysteresis in a fractured rock mass. *International Journal of Rock Mechanics and Mining Sciences* 37(1-2):89–106
- Gérard A, Baumgärtner J, Baria R, Jung R (1997) An attempt towards a conceptual model derived from 1993 to 1996 hydraulic operations at Soultz. In: Paper presented at NEDO International Geothermal Symposium, 11–12 March 1997, Sendai, Japan.
- Haas J, Hoffmann C (1929) Temperature gradient in Pechelbronn oil-bearing region, Lower Alsace: its determination and relation to oil reserves. *Bull Am Assoc Petr Geol* 13:1257–1272

- Held S, Genter A, Kohl T, Kolbel T, Sausse J, Schoenball M (2014) Economic evaluation of geothermal reservoir performance through modeling the complexity of the operating EGS in Soultz-sous-Forêts. *Geothermics* 51:270–280
- Hettkamp T, Fuhrmann G, Rummel F (1999) Hydraulic properties in the Rhine Graben basement material. *Bulletin d'Hydrogéologie Centre d'Hydrogéologie, Université de Neuchâtel* 17:143–150
- Hooijkaas GR, Genter A, Dezayes C (2006) Deep-seated geology of the granite intrusions at the Soultz EGS site based on data from 5 km-deep boreholes. *Geothermics* 35(5-6):484–506
- Huenges E (ed) (2010) *Geothermal Energy Systems*. Wiley-VCH
- Huenges E, Hurter S (2002) In-situ Geothermielabor Groß Schönebeck 2000/2001: Bohrarbeiten, Bohrlochmessungen, Hydraulik, Formationsfluide, Tonminerale. Scientific Technical Report 02/14. Tech. rep., Geoforschungszentrum Potsdam, Germany.
- International Energy Agency (2009) Energy statistics of Non-OECD countries. Tech. rep.
- Ito T, Zoback MD (2000) Fracture permeability and in situ stress to 7 km depth in the KTB Scientific Drillhole. *Geophysical Research Letters* 27(7):1045–1048
- Kohl T, Evans KF, Hopkirk RJ, Rybach L (1995) Coupled hydraulic, thermal and mechanical considerations for the simulation of hot dry rock reservoirs. *Geothermics* 24(3):345–359
- Kolditz O (1997) *Strömung, Stoff- und Wärmetransport im Kluftgestein*. Borntraeger-Verlag, Berlin-Stuttgart
- Kolditz O, Blöcher G, Clauser C, Diersch HJ, Kohl T, Kühn M, McDermott C, Wang W, Watanabe N, Zimmermann G (2010) *Geothermal Energy Systems*, Wiley-VCH, chap Geothermal Reservoir Simulation, pp 245–302
- Kolditz O, Görke UJ, Shao H, Wang W (2012) Thermo-hydro-mechanical-chemical processes in fractured porous media. *Lecture Notes in Computational Science and Engineering* 86 LNCSE:1–404
- Kolditz O, Shao H, Wang W, Bauer S (2015) Thermo-hydro-mechanical-chemical processes in fractured porous media: Modelling and benchmarking - closed form solutions. *Terrestrial Environmental Sciences* 1 TES:1–315
- Kwiatak G, Bohnhoff M, Dresen G, Schulze A, Schulte T, Zimmermann G, Huenges E (2010) Microseismicity induced during fluid-injection: A case study from the geothermal site at Groß Schönebeck, North German Basin. *Acta Geophysica* 58(6):995–1020
- Le Carlier C, Royer JJ, Flores E (1994) Convective heat transfer at the Soultz-sous-Forêts geothermal site: implications for oil potential. *First Break* 12(11):553–560
- Magri F, Bayer U, Jahnke C, Clausnitzer V, Diersch HJ, Fuhrman J, Moller P, Pekdeger A, Tesmer M, Voigt HJ (2005) Fluid-dynamics driving saline water in the North East German Basin. *International Journal of Earth Sciences* 94(5-6):1056–1069

- McDermott C (2006) Reservoir engineering and system analysis: Hydraulic, thermal and geomechanical coupled processes in geosystems. Habilitation, Faculty for Geoscience, Eberhard Karls Universität Tübingen, Germany.
- Moeck I, Kwiatek G, Zimmermann G (2009) Slip tendency analysis, fault reactivation potential and induced seismicity in a deep geothermal reservoir. *Journal of Structural Geology* 31(10):1174–1182
- Nishida A (2010) Experience in developing an open source scalable software infrastructure in japan. In: Taniar D, Gervasi O, Murgante B, Pardede E, Apduhan BO (eds) *Computational Science and Its Applications – ICCSA 2010: International Conference, Fukuoka, Japan, March 23-26, 2010, Proceedings, Part II*, Springer Berlin Heidelberg, Berlin, Heidelberg, pp 448–462
- Noorishad J, Tsang CF (1996) Coupled thermohydroelasticity phenomena in variably saturated fractured porous rocks – formulation and numerical solution. In: Ove Stephansson LJ, Tsang CF (eds) *Coupled Thermo-Hydro-Mechanical Processes of Fractured Media - Mathematical and Experimental Studies*, vol 79, Elsevier, pp 93–134
- O’Sullivan MJ, Pruess K, Lippmann MJ (2001) State of the art of geothermal reservoir simulation. *Geothermics* 30(4):395–429
- Pfender M, Nami P, Tischner T, Jung R (2006) Status of the Soultz deep wells based on low rate hydraulic tests and temperature logs. In: *EHDRA Scientific Conference*, 15–16 June 2006, Soultz-sous-Forêts, France.
- Place J, Sausse J, Marthelot JM, Diraison M, Geraud Y, Naville C (2011) 3-D mapping of permeable structures affecting a deep granite basement using isotropic 3C VSP data. *Geophysical Journal International* 186(1):245–263
- Ramey HJ, Brigham W, Chen H, Atkinson P, Aihara N (1974) Thermodynamic and hydrodynamic properties of hydrothermal systems. In: *Proceedings of an NSF conference on "The Utilization of Volcano Energy"*, Hilo, Hawaii
- Rutqvist J, Stephansson O (2003) The role of hydromechanical coupling in fractured rock engineering. *Hydrogeology Journal* 11(1):7–40
- Sanjuan B, Pinault JL, Rose P, Gerard A, Brach M, Braibant G, Crouzet C, Foucher JC, Gautier A, Touzelet S (2006) Tracer testing of the geothermal heat exchanger at Soultz-sous-Forêts (France) between 2000 and 2005. *Geothermics* 35(5-6):622–653
- Sanjuan B, Millot R, Dezayes C, Brach M (2010) Main characteristics of the deep geothermal brine (5 km) at Soultz-sous-Forêts (France) determined using geochemical and tracer test data. *Comptes Rendus Geoscience* 342(7-8):546–559
- Sardini P, Ledésert B, Touchard G (1997) *Fluid Flow and Transport in Rocks*, Chapman & Hall, London, Great Britain, chap Quantification of microscopic porous networks by image analysis and measurements of permeability in the Soultz-sous-Forêts granite (Alsace, France), pp 171–189

- Sausse J, Fourar M, Genter A (2006) Permeability and alteration within the Soultz granite inferred from geophysical and flow log analysis. *Geothermics* 35(5-6):544–560
- Sausse J, Dezayes C, Dorbath L, Genter A, Place J (2010) 3D model of fracture zones at Soultz-sous-Forêts based on geological data, image logs, induced microseismicity and vertical seismic profiles. *Comptes Rendus Geoscience* 342(7-8):531–545
- Schindler M, Nami P, Schellschmidt R, Teza D, Tischner T (2008) Summary of hydraulic stimulation operations in the 5 km deep crystalline HDR/EGS reservoir at Soultz-sous-Forêts. In: 33rd Workshop on Geothermal Reservoir Engineering, 28–30 January 2008. Stanford University, CA, USA.
- Segura JM, Carol I (2004) On zero-thickness interface elements for diffusion problems. *International Journal for Numerical and Analytical Methods in Geomechanics* 28(9):947–962
- Si H (2015) TetGen, a Delaunay-based quality tetrahedral mesh generator. *ACM Trans on Mathematical Software* 41(2):11:1–11:36
- Snow DT (1969) Anisotropic permeability of fractured media. *Water Resources Research* 5(6):1273–1289
- Trautwein U, Huenges E (2005) Poroelastic behaviour of physical properties in Rotliegend sandstones under uniaxial strain. *International Journal of Rock Mechanics and Mining Sciences* 42(7-8):European Commission
- Watanabe N, Wang W, McDermott C, Taniguchi T, Kolditz O (2010) Uncertainty analysis of thermo-hydro-mechanical coupled processes in heterogeneous porous media. *Computational Mechanics* 45(4):263–280
- Wolfgramm M, Seibt A, Hurter S, Zimmermann G (2003) Origin of geothermal fluids of Permo-Carboniferous rocks in the NE German basin (NE Germany). *Journal of Geochemical Exploration* 78-9:127–131
- Woodbury A, Zhang K (2001) Lanczos method for the solution of groundwater flow in discretely fractured porous media. *Advances in Water Resources* 24(6):621–630
- Ziegler PA (1994) Cenozoic rift system of Western and Central Europe: An overview. *Geologie En Mijnbouw* 73(2-4)
- Zimmerman RW, Bodvarsson GS (1996) Hydraulic conductivity of rock fractures. *Transport in Porous Media* 23:1–30
- Zimmermann G, Reinicke A (2010) Hydraulic stimulation of a deep sandstone reservoir to develop an enhanced geothermal system: Laboratory and field experiments. *Geothermics* 39(1):70–77
- Zimmermann G, Tischner T, Legarth B, Huenges E (2009) Pressure-dependent production efficiency of an Enhanced Geothermal System (EGS): Stimulation results and implications for hydraulic fracture treatments. *Pure and Applied Geophysics* 166(5-7):1089–1106
- Zimmermann G, Moeck I, Blöcher G (2010) Cyclic waterfrac stimulation to develop an Enhanced Geothermal System (EGS) - conceptual design and experimental results. *Geothermics* 39(1):59–69

Zyvoloski G, Dash Z, Kelkar S (1988) FEHM: Finite element heat and mass transfer code. Tech. Rep. LA-11224-MS, Los Alamos National Laboratory